Nucleic Acids Research, 2022 **1**
https://doi.org/10.1093/nar/gkac885

Integrated multi-omics approach revealed cellular senescence landscape

Qiao Song[1], Yuli Hou[1], Yiyin Zhang[2], Jing Liu[1], Yaqi Wang[1], Jingxuan Fu[1], Chi Zhang[1], Min Cao[3], Yuting Cui[1], Xiaomin Zhang[1], Xiaoling Wang[1], Jingjing Zhang[1], Congcong Liu[1], Yingzhen Zhang[1] and Peichang Wang[1,*]

[1]Department of Clinical laboratory, Xuanwu Hospital, National Clinical Research Center for Geriatric Diseases, Capital Medical University, Beijing 100053, PR China, [2]Shanghai Jiayin Biotechnology, Shanghai 200092, PR China and [3]Department of Clinical Laboratory, Beijing Huairou Hospital, Beijing 101400, PR China

Received May 11, 2022; Revised August 27, 2022; Editorial Decision September 27, 2022; Accepted October 01, 2022

ABSTRACT

Cellular senescence is a complex multifactorial biological phenomenon that plays essential roles in aging, and aging-related diseases. During this process, the senescent cells undergo gene expression altering and chromatin structure remodeling. However, studies on the epigenetic landscape of senescence using integrated multi-omics approaches are limited. In this research, we performed ATAC-seq, RNA-seq and ChIP-seq on different senescent types to reveal the landscape of senescence and identify the prime regulatory elements. We also obtained 34 key genes and deduced that NAT1, PBX1 and RRM2, which interacted with each other, could be the potential markers of aging and aging-related diseases. In summary, our work provides the landscape to study accessibility dynamics and transcriptional regulations in cellular senescence. The application of this technique in different types of senescence allows us to identify the regulatory elements responsible for the substantial regulation of transcription, providing the insights into molecular mechanisms of senescence.

INTRODUCTION

Cellular senescence (or merely 'senescence') is a cell fate that includes permanent cell cycle arrest, expression of senescence-associated transcripts (e.g. p16INK4a and NF-kB), and acquisition of a senescence-associated secretory phenotype (1). Senescent cells occur throughout life and play beneficial roles in various physiological processes, including embryo development, tissue repair, and tumor suppression (1,2). Meanwhile, the steady accumulation of senescent cells in key cellular niches that occur with age also has adverse consequences, which could drive aging and aging-related diseases.

Over the past decades, many epigenomic studies focused on cellular senescence and explored novel approaches to identify, characterize, and eliminate senescent cells (3–7). During senescence, the cells that finally succumb to multifactorial stress undergo alterations in the general loss of histones coupled with local and global chromatin remodeling, an imbalance of activating, repressive histone modifications, and global transcriptional change (8,9). However, information on how epigenetic alterations specifically regulate transcriptional changes and gene expression is still limited.

In this study, we used an integrated multi-omics approach comprising assays of transposase-accessible chromatin (ATAC-seq), RNA-seq and ChIP-seq to reveal the landscape of senescence and identify the prime regulatory elements and key genes. We chose different types of stress-induced senescence, which were including replicative cellular senescence (RS) and oncogene induced senescence (OIS, which often been mutant at $HRAS^{v12}$), to reveal the substantial changes and elucidate the characteristics of senescence.

MATERIALS AND METHODS

Cell culture

Human diploid 2BS fibroblasts cells were grown in minimum essential medium (Gibco, 11095080) supplemented with 10% certified fetal bovine serum (BI, 04-001-1A), 1% 200 mM glutamine (Gibco, A2916801), 1% 10000 U/ml Penicillin–Streptomycin (Gibco, 15140122), and 1% MEM non-essential amino acids (Gibco, 11140050), in a humidified atmosphere with 5% CO_2 at 37°C. These cells were considered as 'growing' at PD30 or below and as 'senescent' at PD50 or above.

*To whom correspondence should be addressed. Tel: +86 10 8319 8688; Fax: +86 10 6301 2833; Email: pcw1905@126.com

ATAC-seq

After 50 000 2BS cells were counted, Tn5 transposase was used to simultaneously cut the hierarchically folded DNA. Native nuclei were purified by MinElute PCR Purification Kit (Qiagen, 28004) and amplified by six cycles of quantitative real-time PCR. Genomic DNA of 10 ng was used as input control.

Data download

The previous publication datasets of ATAC-seq, RNA-seq and ChIP-seq were downloaded from GEO database (https://www.ncbi.nlm.nih.gov/geo/). The GSM IDs of them in this assay are listed in Supplementary Table S1.

ATAC-seq and ChIP-seq data processing

ATAC-seq and ChIP-seq libraries were sequenced on the Illumina Hiseq PE150 sequencer or other platform to obtain 60–130 million of 2 × 150 bp paired-end sequencing reads per sample. Data quality was controlled using FastQC (v.0.11.9, www.bioinformatics.babraham.ac.uk/projects/fastqc). After trimming the adaptor and removing low-quality reads, the obtained clean data were aligned to human genome hg38 by the Burrows–Wheeler Aligner tool (v.0.7.10). A peak calling analysis was conducted using MASC2 (v.2,2) with the following parameters: macs2 callpeak -nomodel -f BAMPE–keep -dup 1 -q 0.05 -B–SPMR. Integrative Genomics Viewer (IGV) (v.2.7.0) was used to track visualization. Only peaks that were consistently observed in replicates were emphasized to identify the Tn5 hypersensitive set region (THSS) region with the highest confidence for each condition. The THSSs were annotated to genomic feature and GC percentage using the annotatePeaks.pl of HOMER (v.4.11) software. Read counts were analyzed by BEDTools, and visualization was performed using 'ggplot2' R packages. Transcription factor binding motifs were identified with HOMER findMotifsGenome.pl tool in the chromatin-accessible region; those with P-value <0.05 were considered significant.

RNA-seq data processing

For RNA-seq, raw data were trimmed by removing the adaptor to construct sequencing libraries. The batch effects were removed by an empirical Bayes framework with the 'ComBat' function in the 'sva' R package. In order to maintain original value of batch adjustment, differentially expressed genes (DEGs) were identified by 'limma' R package; those with P-value < 0.05 and abs ($\log_2$FC) >0.26 were considered significant.

Correlation between chromatin accessibility and gene expression

In order to assess the global relationship between chromatin accessibility and gene expression, we categorized the genes into high, medium and low. The threshold of three quantile chromatin accessibility groups was determined by ATAC-seq signals. The threshold of three quantile gene expression groups was determined by mRNA level. The heatmap and its clusters (by k-means) were generated with the 'deepTools' R package. The correlated genes were visualized by the 'ggplot2' R package.

Correlation between chromatin accessibility and chromatin characterization

Chromatin state was calculated by chromatin state segmentation (ChromHMM), and the THSSs were classified by different histone post-translational modifications (hPTMs) as follows: unspecific (high enrichment level in all hPTMs), TSS-like (transcription start site like region) (obtained enrichment in H3K4me3, depleting in H3K27me3), enhancer-like (enriched in H3K4me1/H3K27ac, depleting in H3K4me3), and depleted-region (low levels of enrichment for all hPTMs).

Gene ontology (GO) and Kyoto Encyclopedia of Genes and Genomes (KEGG) pathway enrichment analysis

GO enrichment annotations were downloaded from NCBI (http://www.ncbi.nlm.nih.gov/), UniProt (http://www.uniprot.org/) and GO (http://www.geneontology.org/). KEGG pathway enrichment annotations were obtained from KEGG (https://www.genome.jp/kegg/) database. Significant GO and KEGG categories were identified by fisher's exact test, and a false discovery rate was used to correct the P-value.

Statistical analysis

All data were presented as mean ± standard deviation. Independent sample t-test was used to compare the two groups. P-value <0.05 indicated statistically significant differences between compared groups. Statistical analyses were performed by GraphPad Prism 6 software and R packages.

Gene Expression Profiling Interactive Analysis (GEPIA)

GEPIA server (http://gepia.cancer-pku.cn/) was used to analyze the data of The Cancer Genome Atlas (TCGA) Program and The Genotype-Tissue Expression (GTEx) Project, including gene correlation, disease-free survival (DFS), and pathological stage. Correlation analysis was conducted using data from the GTEx database, including adipose, adrenal gland, bladder, Epstein–Barr virus-transformed lymphocytes, artery, whole blood, leukemia cell line, brain, breast, cervix, colon, esophagus, fallopian tubes, heart, kidneys, liver, lungs, muscles, nerves, ovaries, pancreas, pituitary gland, prostate gland, minor salivary gland, transformed fibroblasts, skin, small intestine, spleen, stomach, testis, thyroid and uterus. The coefficient was calculated on a non-log scale using Pearson correlation, and a log scale axis was applied for visualization. DFS was analyzed by log-rank test using the TCGA database composed of 33 cancer types, namely, adrenocortical carcinoma (ACC), bladder urothelial carcinoma (BLCA), breast invasive carcinoma (BRCA), cervical squamous cell carcinoma and endocervical adenocarcinoma (CESC), cholangiocarcinoma (CHOL), colon adenocarcinoma (COAD), lymphoid neoplasm diffuse

large B-cell lymphoma (DLBC), esophageal carcinoma (ESCA), glioblastoma multiforme (GBM), head and neck squamous cell carcinoma (HNSC), kidney chromophobe (KICH), kidney renal clear cell carcinoma (KIRC), kidney renal papillary cell carcinoma (KIRP), acute myeloid leukemia (LAML), brain lower grade glioma (LGG), liver hepatocellular carcinoma (LIHC), lung adenocarcinoma (LUAD), lung squamous cell carcinoma (LUSC), mesothelioma, ovarian serous cystadenocarcinoma (OV), pancreatic adenocarcinoma (PAAD), pheochromocytoma and paraganglioma, prostate adenocarcinoma, rectum adenocarcinoma (READ), sarcoma (SARC), skin cutaneous melanoma (SKCM), stomach adenocarcinoma (STAD), testicular germ cell tumor (TGCT), thyroid carcinoma (THCA), thymoma (THYM), uterine corpus endometrial carcinoma (UCEC), uterine carcinosarcoma (UCS) and uveal melanoma. The pathological stage was examined using the following data from the TCGA database: ACC, BLCA, BRCA, CESC, CHOL, COAD, DLBC, ESCA, GBM, HNSC, KICH, KIRC, KIRP, LAML, LGG, LIHC, LUAD, LUSC, OV, PAAD, READ, SARC, SKCM, STAD, TGCT, THCA, THYM, UCEC and UCS. DEGs were analyzed by one-way ANOVA using the pathological stage as a variable for calculating differential expression. Expression data were first $\log_2$ (TPM + 1) transformed for differential analysis.

Participants

Volunteers consisting of healthy people (n = 60, with no restriction of age), young healthy people (n = 20, age = 25.3 ± 1.53 years), old healthy people (n = 20, age = 73.25 ± 2.22 years), patients who suffered from stroke (n = 20, age = 74.65 ± 3.30 years), patients with Pan-Cancer (n = 20, age = 73.05 ± 2.86 years), and patients with diabetes (n = 20, age = 75.2 ± 2.33 years) donated their peripheral blood with informed consent. All participants were non-smokers, and the healthy people were free from history of recent infection, chronic disease, or any medication supplementation for 4 weeks prior to the experiment. The study was approved by the ethics board of Xuanwu hospital Capital Medical University.

Collected whole blood samples and isolated peripheral blood mononuclear cells (PBMCs)

Fresh peripheral blood samples were collected in Vacutainer® Plus Plastic EDTA-K_2 tubes (BD, 367862). PBMCs were isolated from the fresh peripheral blood by density gradient centrifugation with Ficoll (TBD, LTS1077) following the experimental protocol. Stroke-physiological saline solution (CR DOUBLE-CRANE, H34023609) was applied to dilute the peripheral blood.

Western blot

The PBMCs were lysed with radioimmunoprecipitation assay lysis buffer (Solarbio, R0010) containing phenylmethanesulfonyl fluoride (Solarbio, P0100) and protease inhibitor cocktail (Beyotime, P1005). The protein concentration of cell lysates was detected by Pierce BCA Protein Assay Kit (Thermo, 23227). Then, the equal concentrations of protein were loaded and run on the 10% SDS-PAGE gel (Beyotime, P0012A) to separate. After transferred to a polyvinylidene fluoride membrane (Millipore, IPVH00010), protein bands were detected by incubating the indicated horseradish peroxidase-conjugated antibodies, including GAPDH (Proteintech, 10494-1-AP), RRM2 (Proteintech, 11661-1-AP), PBX1 (Proteintech, 18204-1-AP), and NAT1 (Proteintech, 19188-1-AP). The bands were visualized by enhanced chemiluminescence (Yeasen, 36222ES60).

Co-immunoprecipitation (Co-IP)

To obtain the clearer bands, the cell extracts amount could range from 100 to 1200 μg. The cell extracts from the PBMCs of healthy people were separately rotated and incubated with 4 μg antibodies of RRM2 (Proteintech, 11661-1-AP), PBX1 (Proteintech, 18204–1-AP), NAT1 (Proteintech, 19188-1-AP), and IgG (Abcam, ab172730) at 4°C for 12 h, followed by incubation with 50 μl (0.50 mg) of PureProteome™ Protein A/G Mix Magnetic Beads (Millipore, LSKMAGAG10) at 4°C for 4 h with rotation. Every 60 μg cell extracts were isolated as input. The magnetic beads were then washed three times with ice-cold extraction buffer, mixed with 1 × protein loading buffer which was diluted by 5× protein loading buffer (LABLEAD, G2527) with extraction buffer, and boiled at 95°C for 10 min. Then, the IP products were loaded and run on the 10% SDS-PAGE gel (Beyotime, P0012A) to separate. After transferred to a polyvinylidene fluoride membrane (Millipore, IPVH00010), protein bands were detected by incubating the indicated horseradish peroxidase-conjugated antibodies, including RRM2 (Proteintech, 11661-1-AP), PBX1 (Proteintech, 18204-1-AP), and NAT1 (Proteintech, 19188-1-AP). The bands were visualized by enhanced chemiluminescence (Yeasen, 36222ES60).

RESULTS

High-resolution chromatin accessibility profiles revealed differences between growing and senescent cells

Considering that human diploid 2BS fibroblasts are a widely used cell model to study cellular senescence and aging-related disorders, we employed growing 2BS cells and senescent 2BS cells as RS representatives to generate ATAC-seq libraries (created with BioRender.com) (Figure 1A), which can sensitively measure high-resolution chromatin accessibility (10,11). For each age stage, we obtained two independent ATAC-seq replicates. To explore any difference in OIS, we also obtained the ATAC-seq data of cellular senescence from GSM2774972, GSM2774973, GSM2774974, control data from GSM2774968, GSM2774969, GSM2774970, GSM2774971 (12). Through the unbiased clustering of all ATAC-seq samples, we observed a correlation between RS and OIS, suggesting their homogeneity (Figure 1B). Principal component analysis (PCA) in RS and OIS groups identified age as the main variation source (Supplementary Figure S1A, B).

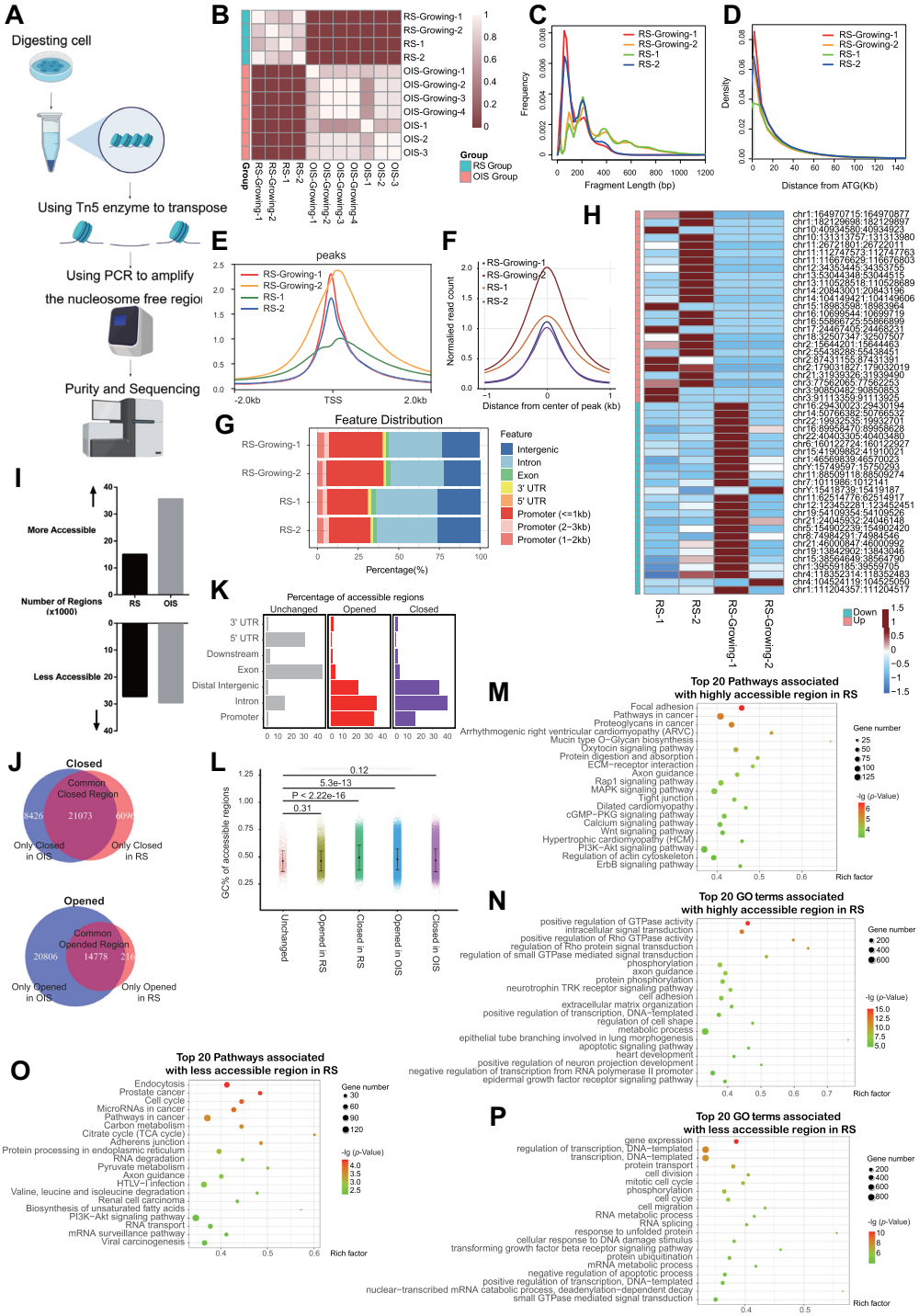

Figure 1. Highresolution chromatin accessibility profiles revealed differences between growing and senescent cells. (**A**) Graphical explanation of ATAC-seq process. (**B**) Unbiased clustering of RS (Replicative Cellular Senescence) cells, OIS (Oncogene Induced Senescence) cells, and corresponding control replicates. This picture was created with 'BioRender.com'. (**C**) Distribution of ATACseq fragment size in RS cells and growing cells. (**D**) The position of THSSs (Tn5 hypersensitive set regions) in RS cells and growing cells can be observed in density plot. Enrichment of ATAC seq signal around the (**E**) TSS (transcription start site) and (**F**) gene center in RS cells and growing cells. (**G**) The annotation of accessible chromatin in Genome can be observed in it, the genomic features including exons, intergenic regions, introns, promoters, 3'UTR, and 5'UTR. (**H**) Heatmap of 50 most enriched ATACseq peaks at accessible chromatin regions in RS cells. (**I**) Numbers of altered accessibility regions can be observed in bar plot. (**J**) Venn diagram revealed the homogeneity and heterogeneity between different types of senescence in terms of chromatin accessibility. (**K**) Annotation of opened and closed accessible regions in RS. (**L**) Genomic GC percentage of the accessible regions. (**M**) Pathways associated with highly accessible chromatin regions in RS cells shown as a bubble chart. The Xaxis was Richfactor, which represents the level of enrichment. The cycle size represents the number of peaks in this GO (gene ontology) term. The color of cycle represents lg(*P*-value). (**N**) GO terms associated with highly accessible chromatin regions in RS cells was shown as a bubble chart. (**O**) Pathways associated with less accessible chromatin regions in RS cells. (**P**) GO terms associated with less accessible chromatin regions in RS cells. The results of OIS could also be seen in Supplementary Figure S1.

The similar distribution of fragment sizes suggested that chromatin was accessible to Tn5 transposase corresponding to integer multiples of nucleosomes in all samples independently of the stage of age (Figure 1C and Supplementary Figure S1C). We also found that the THSS regions were mostly located from 2 kb upstream of the translation start codon (ATG) to 2 kb downstream of the nearest gene (Figure 1D and Supplementary Figure S1D). Moreover, we observed the strong enrichment of ATAC-seq reads around TSS and the enrichment of ATAC-seq signal around the gene center (Figure 1E, F and Supplementary Figure S1E, F).

Based on these observations, we annotated the peaks to explore the position of accessible chromatin in the genome and found that the chromatin accessibility around the promoter region in growing cells was higher than that in senescent cells (Figure 1G and Supplementary Figure S1G). According to the genomic distribution of peaks, the number of promoter-enriched peaks of senescent cells was significantly higher than that of growing cells, whether in RS or OIS. The heatmap of ATAC-seq in Figure 1H and Supplementary Figure S1H lists the most enriched genes in senescent cells.

Using MACS2 peak calling, we also performed differential binding analysis to quantitatively identify the regions of altered accessibility. We observed 14,994 regions that were significantly more accessible (opened) and 27 169 regions that were significantly less accessible (closed) in RS cells compared with that in growing cells (Figure 1I). For OIS cells, 35 584 regions were more accessible, and 29 499 regions were less accessible. We found that chromatin accessibility was relatively closed in RS cells (compared with control) but relatively open in OIS cells. Although RS differed from OIS in chromatin accessibility alteration, they shared a few overlapped genes that were enriched in altered regions (Figure 1J).

After peak annotation by HOMER, we found that the accessible regions altered in RS and OIS cells were enriched at distal intergenic, intronic, and promoter regions (Figure 1K and Supplementary Figure S1I). We used BEDTools to explore the relationship between chromatin accessibility and GC richness and found that the less accessible regions in RS cells and the highly accessible regions in OIS showed significant GC richness and AT poorness, respectively (Figure 1L). However, the else regions showed no significant differences (opened in RS or closed in OIS).

As we known cellular senescence is closely related to numerous genes that participate in multiple signaling pathways (3). To explore the role of chromatin-accessible regions in gene function and in the regulation of genes involved in signaling pathways, we analyzed different pathways and biological processes in growing cells and different types of senescent cells.

We found that the opened regions in RS were enriched in various signaling pathways, including focal adhesion, mucin-type O-glycan biosynthesis, and oxytocin signaling pathway, which played essential roles in hyperplastic pathologies and degenerative pathologies (Figure 1M) (13–15). This finding was analogous to the enrichment of opened regions in OIS (Supplementary Figure S1J). The loss of cell proliferation and the increased level of glycosylation in cellular senescence may account for some of the above changes in the signaling pathway (2,16). GO analysis revealed that several aging-associated biological processes, such as GTPase activity, intracellular signal transduction, and Rho-GTPase activity, were upregulated in RS and OIS (Figure 1N and Supplementary Figure S1K). Transcription plays a key role in senescence, whether in RS or OIS, which consisted with previous studies (17–19).

We also found that the closed regions in RS were enriched in several pathways, including endocytosis, cell cycle, and carbon metabolism; this finding was in line with the enrichment of closed regions in OIS (Figure 1O and Supplementary Figure S1L). Several factors, such as cell cycle alteration, dysfunctional endocytic components and so forth, also play a strong part in senescence (2,20). GO analysis showed that several aging-associated biological processes, including gene expression, transcription, and protein transport, were downregulated in RS and OIS (Figure 1P and Supplementary Figure S1M).

Gene expression profiles revealed differences between growing and senescent cells

After observing the chromatin accessibility of senescent cells, we focused on the expression difference between growing and senescent cells. Thus, we analyzed the RNA-seq data of RS cells from GSM1290017, GSM1290018, GSM1553104, GSM1553105, GSM1553109, GSM1553110, GSM1553111, GSM2595526, GSM2595527, GSM2828806 and GSM2828808, we obtained control from GSM1290015, GSM1290016, GSM1553101, GSM1553102, GSM1553106, GSM1553107, GSM1553108, GSM2595515, GSM2595516, GSM2828805 and GSM2828807 (21–26). We also obtained the RNA-seq data of OIS cells from GSM2828815, GSM2828816, GSM2786639, GSM2786646, GSM2786653, GSM1861913, GSM1861914, GSM1861915, GSM1861916, GSM1861917, GSM1861918 and the control data from GSM2828805, GSM2828807, GSM2786635, GSM2786642, GSM2786649, GSM1035443, GSM1035444, GSM1861907, GSM1861908, GSM1861909, GSM1861910, GSM1861911, GSM1861912 (12,26–28).

After normalization and batch effects removal, we performed PCA analysis to determine the main variation source across the expression of RS and OIS groups (Figure 2A and Supplementary Figure S2A). Through the unbiased clustering of all RNA-seq samples, we observed a correlation between RS and OIS, suggesting their homogeneity (Figure 2B).

Through identification by 'limma', we found that gene expression differed significantly between senescent and growing cells. The number of upregulated and downregulated genes was 507 and 935 from RS cells, respectively, and 605 and 183 from OIS cells (Figure 2C and Supplementary Figure S2B). The heatmap of RNA-seq in Figure 2D (RS cells) and Supplementary Figure S2C (OIS cells) lists the genes with the most altered expression in senescent cells (Figure 2D, Supplementary Figure S2C).

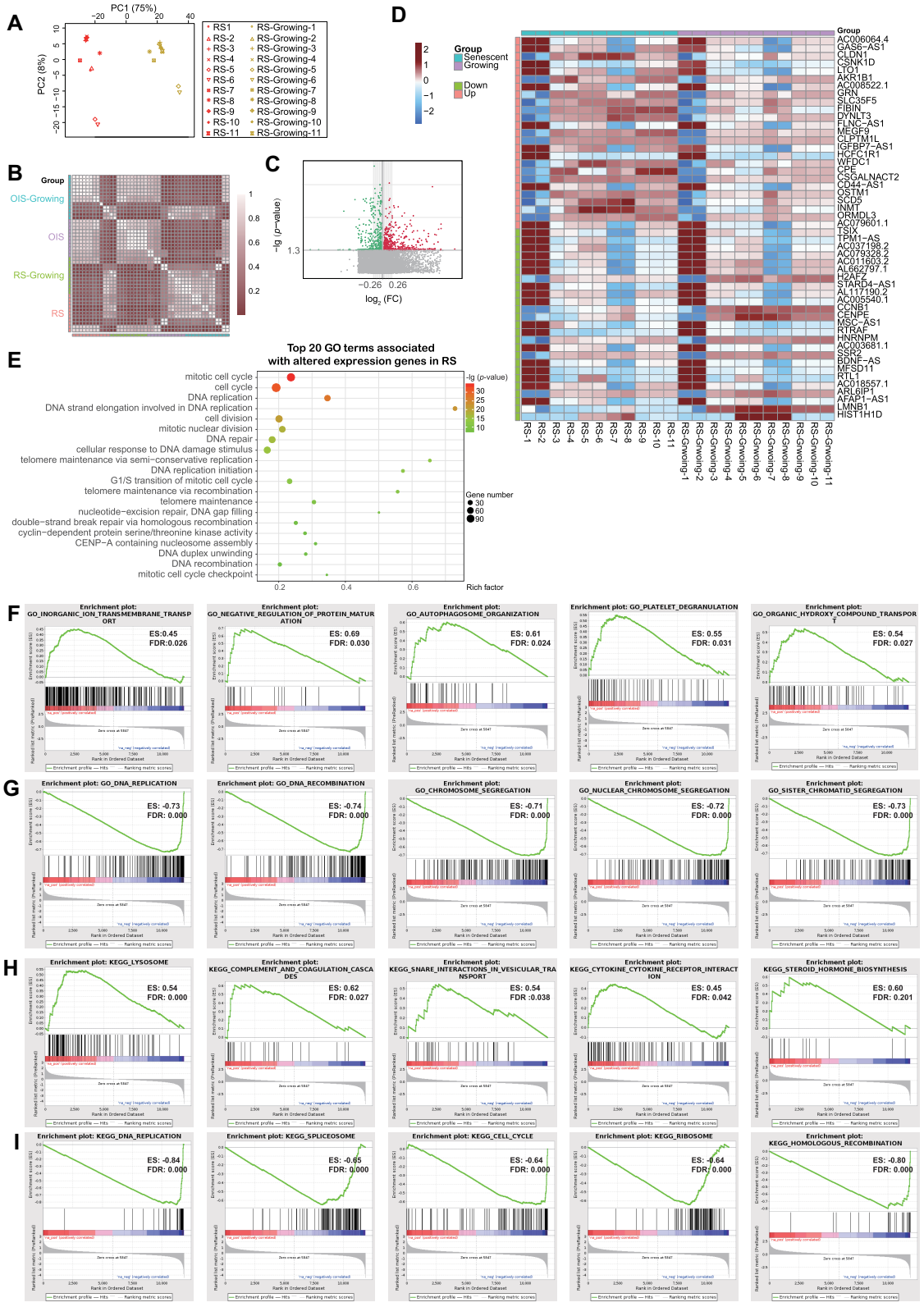

Figure 2. Gene expression profiles revealed differences between growing and senescent cells. (**A**) PCA (Principal com ponent analysis) analysis of RS cells can be observed indicated. (**B**) Unbiased clustering of RS cells, OIS cells, and corresponding control replicates. (**C**) Differentially expressed genes of RS cells were shown as a volcano plot, in which upregulated genes are indicated by red dots, and downregulated genes are indicated by green dots. (**D**) Heatmap of the 50 genes with the most altered expression in RS cells. (**E**) GO terms associated with the expression of altered genes in RS cells. (**F**) Top 5 GO biological processes associated with upregulated genes in RS cells revealed by GSEA (Gene Set Enrichment Analysis) algorithm. (**G**) Top 5 GO biological processes associated with downregulated genes in RS cells revealed by GSEA algorithm. (**H**) Top 5 pathways associated with upregulated genes in RS cells revealed by GSEA algorithm. (**I**) Top 5 pathways associated with downregulated genes in RS cells revealed by GSEA algorithm. The results of OIS could also be seen in Supplementary Figure S2.

Consistent with the literature, the altered genes (whether in RS or OIS) were significantly enriched in several GO terms such as cell cycle, DNA replication, and DNA repair (19,29) (Figure 2E, Supplementary Figure S2D). To distinguish the core biological process, we used the Gene Set Enrichment Analysis (GSEA) algorithm to calculate gene enrichment in GO-BP items (30). We found that the upregulated genes were enriched in biological processes such as ribosome biogenesis (ES: 0.54, FDR: 0.000), rRNA metabolic process (ES: 0.52, FDR: 0.000), ncRNA metabolic process (ES: 0.48, FDR: 0.000), inorganic ion transmembrane transport (ES: 0.45, FDR: 0.026), negative regulation of protein maturation (ES: 0.69, FDR: 0.030), autophagosome organization (ES: 0.61, FDR: 0.024) and so on (Figure 2F, Supplementary Figure S2E). Meanwhile, the downregulated genes were enriched in biological processes such as sister chromatid cohesion (ES: −0.72, FDR: 0.000), sister chromatid segregation (ES: −0.69, FDR: 0.000), nuclear chromosome segregation (ES: −0.68, FDR: 0.000), DNA replication (ES: −0.73, FDR: 0.000), DNA recombination (ES: −0.74, FDR: 0.000), chromosome segregation (ES: −0.71, FDR: 0.000) and so on (Figure 2G, Supplementary Figure S2F). To focus on the key pathways in senescence, we used GSEA and found that the upregulated genes were enriched in pathways such as lysosome (ES: 0.54, FDR: 0.000), complement and coagulation cascades (ES: 0.62, FDR: 0.027), snare interactions in vesicular transport (ES: 0.54, FDR: 0.038), ribosome (ES: 0.50, FDR: 0.026), natural killer cell mediated cytotoxicity (ES: 0.52, FDR: 0.034), VEGF signaling pathway (ES: 0.53, FDR: 0.028) and the like (Figure 2H, Supplementary Figure S2G). Meanwhile, the downregulated genes were enriched in pathways including DNA replication (ES: −0.84, FDR: 0.000), spliceosome (ES: −0.65, FDR: 0.000), cell cycle (ES: −0.64, FDR: 0.000), ECM receptor interaction (ES: −0.61, FDR: 0.003), homologous recombination (ES: −0.80, FDR: 0.000), oocyte meiosis (ES: −0.55, FDR: 0.000) and so on (Figure 2I, Supplementary Figure S2H).

Association between chromatin accessibility and gene expression in senescence

It is universally acknowledged that chromatin accessibility may have been correlated with gene expression (31). To explore this relationship, we labeled the RNA-seq signals as low, medium, or high and then categorized ATAC-seq data as matched RNA-seq signals to calculate the enrichment in TSS regions. The violin diagram revealed that the highly transcribed genes possessed more open chromatin landscapes than the genes with low transcriptional levels, whether in RS, OIS, or the control group (Figure 3A, B and Supplementary Figure S3A, B). We also assigned the regions of altered accessibility (opened or closed in RS or OIS) to nearby genes and matched them with gene expression signals, reaching the same conclusion (Figure 3C). We constructed a Venn diagram to illustrate the association between chromatin accessibility and gene expression. In RS, 1725 genes were associated with the altered chromatin accessibility, 1442 genes were associated with the altered expression, and 98 genes were associated with the altered chromatin accessibility and expression (Figure 3D). In OIS, 5111 genes were associated with the altered chromatin accessibility, 726 genes were associated with the altered expression, and 69 genes were associated with the altered chromatin accessibility and expression (Figure 3D).

The heatmap of both altered genes in Figure 3E (RS cells) and Supplementary Figure S3C (OIS cells) lists the top 50 altered genes in senescent cells. In RS, the simultaneously increasing genes included ATP2C2, BCAS3, CREG1, DYNC1I1, OAS2, OPRL1, PDE11A, PPFIBP2, RAI2, SYT17 and TNFSF13B (Figure 3F), the simultaneously decreasing genes included RRM2, ACSS1, DMC1, HEY1, HTR1B, SLC25A10, ZNF214 and so on (Figure 3G). In OIS, the simultaneously increasing genes included C1ORF147, IL1B, SERPINB4, TNFSF8, WTAPP1 and so on (Figure 3H), the simultaneously decreasing genes included FPGT, GRIK2, GUCY1B1, ID2, KIAA0895, NAT1, PBX1, PLA2G12A, ROBO2, PRSS35 and SLIT2 (Figure 3I).

We also explored the enrichment of chromatin accessibility and altered gene expression in pathways. Consistent with the findings in the previous section, the altered genes were significantly enriched in several pathways such as cell cycle, DNA replication, DNA repair and cellular senescence (Figure 3J and Supplementary Figure S3D).

Characterization of epigenetic factors in senescence

As mentioned above, the impact of altered chromatin on cellular senescence can partly be attributed to gene expression change. To characterize senescence, we employed specific hPTMs, including H3K4me1, H3K4me3, H3K27ac and H3K27me3, to investigate the features of epigenetic factors in senescence. We obtained RS cells' ChIP-seq data of H3K4me1 from GSM2830417 and GSM2830418, employed control from GSM2830415 and GSM2830416 (26). We obtained OIS cells' ChIP-seq data of H3K4me1 from GSM2775005, GSM2775006, and GSM2775007, employed control from GSM2775000, GSM2775001, GSM2775002 and GSM2775003 (12). We obtained RS cells' ChIP-seq data of H3K4me3 from GSM897560 and employed control from GSM897556 (32). We obtained OS cells' ChIP-seq data of H3K4me3 from GSM1922391, GSM1074459 and GSM1035438, employed control from GSM1922387, GSM1074457, and GSM1035429 (28,33,34). We obtained RS cells' ChIP-seq data of H3K27ac from GSM2830429 and GSM2830430, employed control from GSM2830427 and GSM2830428 (26). We obtained OIS cells' ChIP-seq data of H3K27ac from GSM2774996, GSM2774997, GSM2774998, GSM2774999, GSM1915115 and GSM2098178, employed control from GSM2774992, GSM2774993, GSM2774994, GSM2774995, GSM1915113, and GSM2098176 (12,35). We obtained RS cells' ChIP-seq data of H3K27me3 from GSM897561 and employed control from GSM897557 (32). We obtained OIS cells' ChIP-seq data of H3K27me3 from GSM1035439 and employed control from GSM1035430 (28).

To validate the enrichment of H3K4me1, H3K4me3, H3K27ac, and H3K27me3 across genes, we arranged the genes as lines and sorted them in descending order based on signal intensity. We found that H3K4me1, H3K4me3,

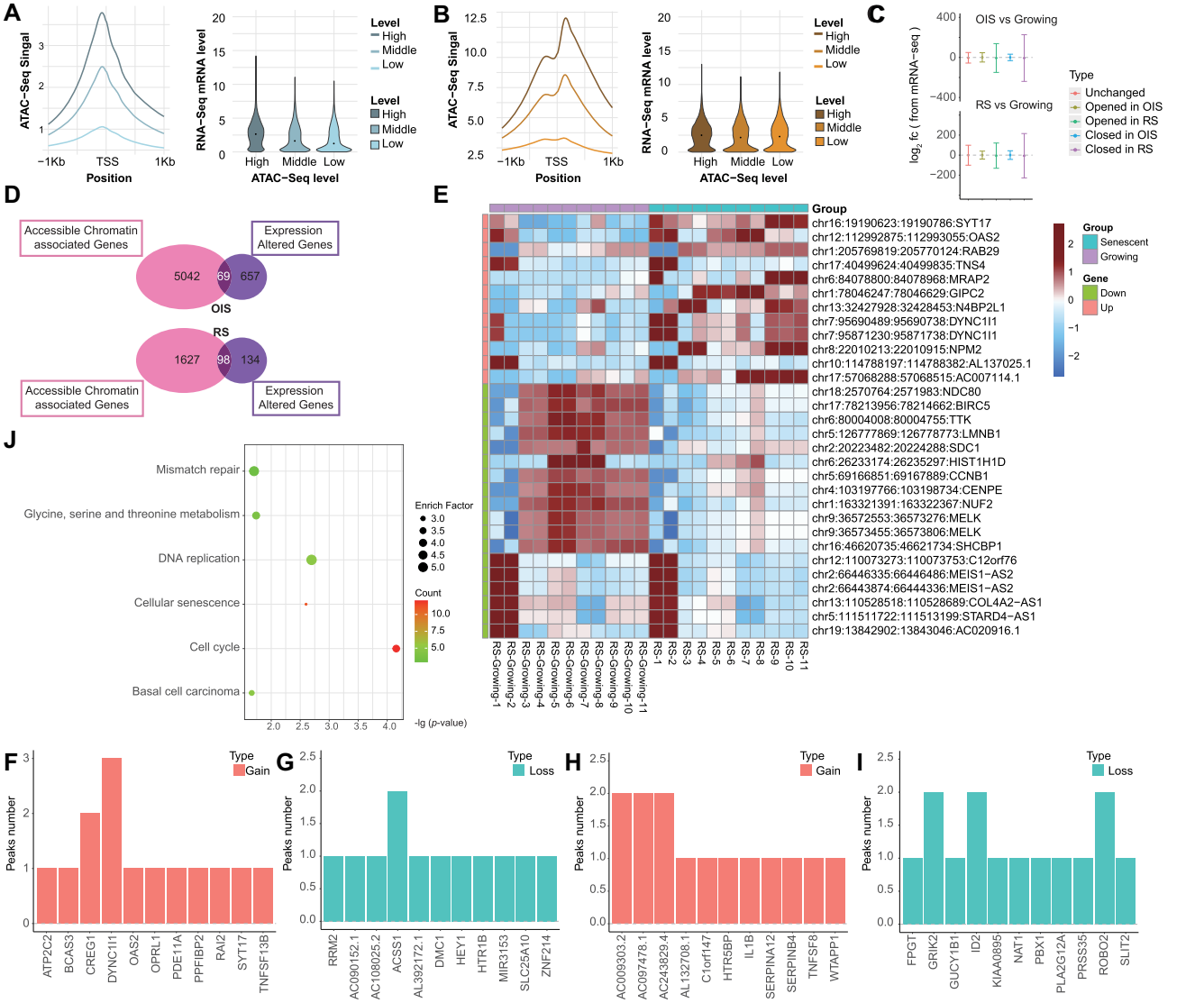

Figure 3. Association between chromatin accessibility and gene expression in senescence. ATACseq signal at TSSs correlates quantitatively with gene expression, (**A**) the left figures (in blue) show the correlation between ATACseq signal at TSS and gene expression in RS cells, (**B**) and the right figures (in brown) show the correlation between ATAC seq signal at TSS and gene expression in growing cells. (**C**) Regions of altered accessibility (opened or closed in RS or OIS) were assigned to nearby genes and matched with gene expression signals. (**D**) Venn diagram showing the genes associated with the chromatinaccessible regions in RS cells and differentially expressed genes. (**E**) Heatmap of the top 50 genes with highest chromatin accessibility and most altered expression in RS cells. (**F**) Upregulated genes in RS that are associated with open chromatin regions. (**G**) Downregulated genes in RS that are associated with open chromatin regions. (**H**) Upregulated genes in OIS that are associated with open chromatin regions. (**I**) Downregulated genes in OIS that are associated with open chromatin regions. (**J**) KEGG (Kyoto Encyclopedia of Genes and Genomes) pathways associated with accessibility and expression of simultaneously altered. The results of OIS could also be seen in Supplementary Figure S3.

H3K27ac and H3K27me3 were less enriched in RS cells; H3K27ac and H3K27me3 were less enriched in OIS cells; and H3K4me1 and H3K4me3 were highly enriched in OIS cells (Figure 4A-D and Supplementary Figure S4A-D). In addition, we found several GO terms enriched in hPTMs, including 'transcription', 'gene expression', 'cell cycle', 'phosphorylation', 'cellular response to DNA damage stimulus', 'translation', 'DNA repair' and so on. These terms were similar to those enriched in ATAC-seq data and RNA-seq data (Figure 4E, G, I, K and Supplementary Figure S4E, G, I, K). The pathways enriched in these epigenetic factors included 'Ubiquitin mediated proteolysis', 'MAPK signaling pathway', 'Calcium signaling pathway', 'Cell cycle', and so on, which were also similar to those enriched in ATAC-seq data and RNA-seq data (Figure 4F, H, J, L and Supplementary Figure S4F, H, J, L).

Association between chromatin accessibility and epigenetic factors modification

It is well-known that regulatory sequences, including TSSs and enhancers, could be a novel and useful marker to identify senescence state (26,36).The regulatory sequences can be distinguished by hPTMs, such as TSS/promoter regions with high enrichment levels for H3K4me3 and low enrichment levels for H3K27me3 and enhancer regions with

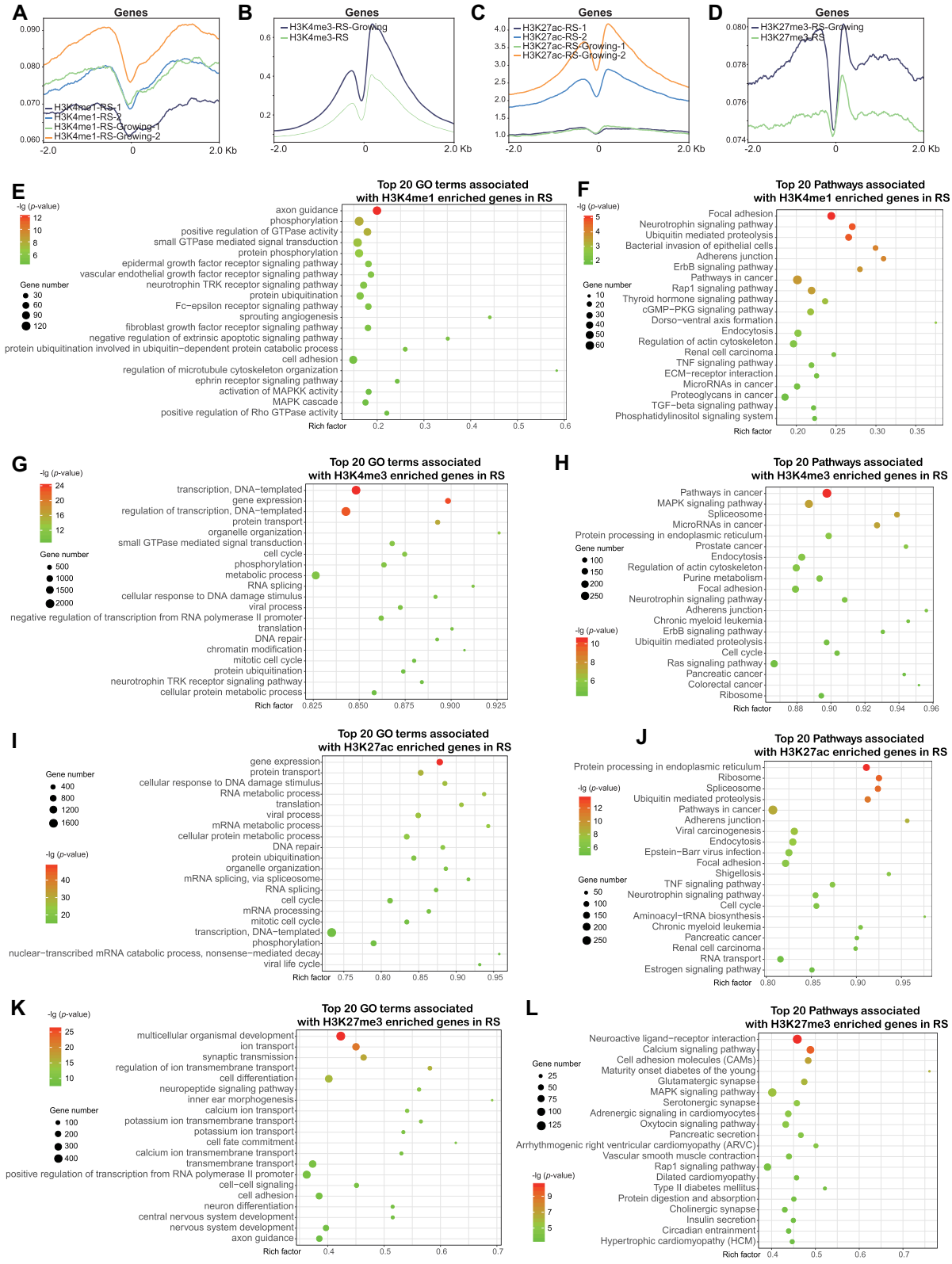

Figure 4. Characterization of epigenetic factors in senescence. (**A**) H3K4me1, (**B**) H3K4me3, (**C**) H3K27ac, (**D**) H3K27me3 distribution around TSS of each RS and control samples, in which the position of TSS were indicated. (**E**) GO terms associated with H3K4me1 enriched genes in RS cells. (**F**) Pathways associated with H3K4me1 enriched genes in RS cells. (**G**) GO terms associated with H3K4me3 enriched genes in RS cells. (**H**) Pathways associated with H3K27ac enriched genes in RS cells. (**I**) GO terms associated with H3K27ac enriched genes in RS cells. (**J**) Pathways associated with H3K27ac enriched genes in RS cells. (**K**) GO terms associated with H3K27me3 enriched genes in RS cells. (**L**) Pathways associated with H3K27me3 enriched genes in RS cells. The results of OIS could also be seen in Supplementary Figure S4.

high enrichment levels for H3K4me1/H3K27ac and low enrichment levels for H3K4me3 (37–42). Based on this assumption, we investigated the association between the THSS of ATAC-seq and the TSS-like or enhancer-like regions identified by hPTMs. We used ChromHMM to partition the genome into four distinct chromatin states according to the relative enrichment of hPTMs: unspecific (enriched in all hPTMs), TSS-like (enriched in H3K4me3 and depleted in H3K27me3), enhancer-like (enriched in H3K4me1, H3K27ac, and depleted in H3K4me3), and depleted (depleted in all hPTMs) (Figure 5A). After that, we overlapped these genomic segments with the THSS regions of ATAC-seq to identify the THSSs with the distinctive features of TSSs and enhancers (Figure 5B-D and Supplementary Figure S5A, B). We found that the THSS regions with TSS-like signatures (identified by hPTMs) were always located within 2 kb of the downstream transcript (Figure 5E and Supplementary Figure S5C). As for rest, we focused on the TSS-like ATAC-seq peaks located 2 kb away from the downstream transcript. In these regions, we found that chromatin accessibility was correlated with gene expression, suggesting that these THSSs are previously unidentified TSSs (Figure 5F and Supplementary Figure S5D).

Integrated multi-omics approach revealed that PBX1, NAT1 and RRM2 could be the new markers of cellular senescence, aging, and aging-related diseases

As stated above, ruling out some ncRNAs (such as AC090152.1, AC108025.2 and MIR3153 etc.) and some less studied genes (such as HTR5BP, SERPINA12 etc., which TCGA and GTEx databases), we found that the following genes were simultaneously altered in ATAC-seq and RNA-seq data and could play a robust part in senescence: ATP2C2, BCAS3, CREG1, DYNC1I1, OAS2, OPRL1, PDE11A, PPFIBP2, RAI2, SYT17, TNFSF13B, RRM2, ACSS1, DMC1, HEY1, HTR1B, SLC25A10, ZNF214, C1ORF147, IL1B, SERPINB4, TNFSF8, WTAPP1, FPGT, GRIK2, GUCY1B1, ID2, KIAA0895, NAT1, PBX1, PLA2G12A, ROBO2, PRSS35 and SLIT2. We called these genes 'Simultaneous-Altered-Genes.' To determine core factors in senescence, aging, and aging-related diseases, we employed the GEPIA server to analyze TCGA and GTEx databases and combined them with our previous ChIP-seq data (43).

The current markers of senescence included CDKN2A, H2AFX, LMNB1, MKI67, POLD1, RB1, TP53 and TP53BP1 (5,17,18,32,44–48). Thus, we focused on the expression correlation between 'Simultaneous-Altered-Genes' and the senescent markers in the GTEx database and used the Pearson correlation method to calculate the correlation coefficient ($P < 0.05$ and $R > 0.3$ indicate correlation). We found that C1ORF147, WTAPP1, NAT1, PBX1, PLA2G12A, FPGT, KIAA0895, BCAS3, CREG1, DYNC1I1, PDE11A, PPFIBP2, TNFSF13B, OAS2, SYT17, RRM2, ACSS1, ZNF214 and DMC1 were significantly correlated with the senescent markers (Figure 6A, Supplementary Figure S6A). The correlations of other 'Simultaneous-Altered-Genes' (which were not correlated with any of the mentioned senescent markers) with senescent markers were shown in Supplementary Figure S6B.

In resent researches, senescent cells have been speculated as a central contributor to aging and aging-related diseases, including various types of cancer (2,49,50)Thus, we focused on the role of 'Simultaneous-Altered-Genes' in cancer. In order to well deciphering the action of senescent cells in cancer, we used GEPIA undertaking 33 cancer types from TCGA to investigate the DFS of 'Simultaneous-Altered-Genes'. In univariable analysis, we found that SERPINB4, TNFSF8, GRIK2, ID2, NAT1, PBX1, PLA2G12A, PRSS35, SLIT2, ATP2C2, BCAS3, CREG1, DYNC1I1, OPRL1, PDE11A, PPFIBP2, RAI2, TNFSF13B, RRM2, ACSS1, SLC25A10 and ZNF214 were the significant variables for the DFS of Pan-Cancer (Figure 6B). The remaining non-significant genes of Pan-Cancer DFS are shown in Supplementary Figure S6C.

We also employed GEPIA to investigate the relationship between 'Simultaneous-Altered-Genes' and Pan-Cancer pathological stages using the data from TCGA and GTEx databases. We found that the expression of almost all 'Simultaneous-Altered-Genes' was statistically significant with the Pan-Cancer pathological stages, except for that of DYNC1I1 and DMC1 (Figure 6C, Supplementary Figure S6D, E).

To unravel the core factors in senescence, we classified the 'Simultaneous-Altered-Genes' into three parts: genes that were correlated with cellular senescence markers (19 genes), those that were statistically significant for Pan-Cancer DFS (22 genes), and those that were statistically significant in Pan-Cancer pathological stage (when F-value was greater than 20) (11 genes). The intersection of the three parts comprised NAT1, PBX1, RRM2 and ZNF214, as shown in Figure 7A. However, no suitable antibody can be found for ZNF214. Hence, we can only use NAT1, PBX1 and RRM2 in further investigations.

Using IGV, we observed the enrichment of ATAC-seq, H3K4me3, H3K27me3, H3K4me1, H3K27ac, TSS-like region (identified by hPTMs and ATAC-seq), and enhancer-like region (identified by hPTMs and ATAC-seq). NAT1 and PBX1 were less enriched in the region around the TSS of senescent cells, and RRM2 was highly enriched in the region around the TSS of senescent cells (Figure 7B and Supplementary Figure S7A).

We employed the group of the healthy people, the stroke patients, the Pan-Cancer patients and the diabetes patients to explore the expression of NAT1, PBX1 and RRM2 in aging and age-related diseases. We found that the expression levels of NAT1 and PBX1 decreased in aging, stroke, Pan-Cancer and diabetes. However, the expression of RRM2 fluctuated with an increase in aging and stroke, a decrease in diabetes, and an insignificant change in Pan-Cancer (Figure 7C–F). Co-immunoprecipitation assay also showed that NAT1, PBX1 and RRM2 could interact with each other and, therefore, could participate in aging and aging-related diseases as protein complexes (Figure 7G).

DISCUSSION

Despite the abundant studies focusing on the alteration of chromatin structure, gene expression, and hPTMs during

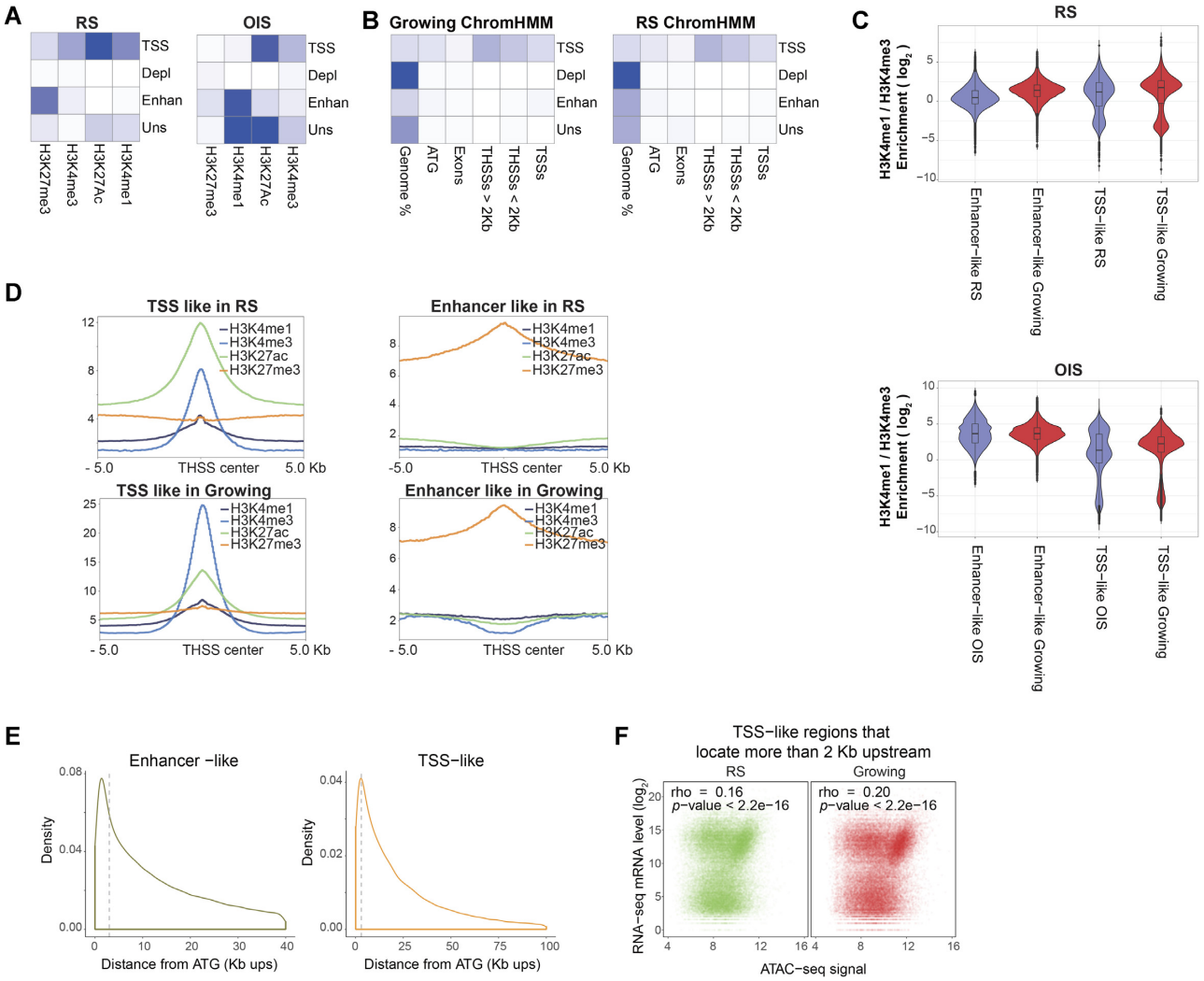

Figure 5. Association between chromatin accessibility and epigenetic factors modification. (**A**) ChromHMM (Chromatin State Segmentation) analysis for a fourchromatinstate model based on hPTMs (histone posttranslational modifications) enrichment patterns presented as heatmaps. The chromatin states were including TSS (enriched in H3K4me3 and depleted in H3K27me3), Depl (depleted in all hPTMs), Enhan (enriched in H3K4me1/H3K27ac and depleted in H3K4me3), and Uns (enriched in all hPTMs). Dark blue indicates the high enrichment of a particular hPTMs. (**B**) Overlap of various genomic features, including THSSs and known TSSs, between RS cells and growing cells shown as heatmaps, in which the predicted chromatin states can also be obtained. Dark blue indicates the high probability of pertinence to a particular chromatin state. (**C**) THSS regions (including TSSlike regions and enhancerlike regions) enrichment in H3K4me1/H3K4me3 was shown as violin plots. Log_2 was used for the ratio scale. (**D**) The RS cells (top) and growing cells (bottom) enrichment of H3K4me1, H3K4me3, H3K27ac and H3K27me3 in THSS regions were shown as average profiles, in which chromatin states were divided into TSS (left) and enhancerlike (right). (**E**) RS cells distribution of distances to the ATG start codon for THSSs characterized as enhancers (left) or TSSlike (right) were shown as density diagrams. (**F**) The RS cells relationship between gene expression and chromatin accessibility at TSSlike regions and enhancerlike regions, which were identified by hPTMs, was shown as scatter plot. ATACseq data and RNAseq data were in the log_2 scale. Spearman rank correlation coefficient (rho) and corresponding *p*value were shown as indicated. The results of OIS could also be seen in Supplementary Figure S5.

cellular senescence, the landscape of senescence at multiple molecular levels remains lacking. In the current study, we provided an integrated multi-omics approach to study different types of cellular senescence, identify the prime regulatory elements and key genes.

Our first objective was to use ATAC-seq, a novel technology that could map nucleosomes and DNA-binding proteins. This method protects sites and is faster, more sensitive, and requires fewer starting materials than other assays to obtain open chromatin regulatory regions in RS and OIS (51). When senescence occurs, the nuclear lamina, heterochromatin, and chromatin connections in senescence are broken down, and the distinction between active and inactive chromatin domains becomes blurred (52). In this research, we revealed the concrete alteration. A robust loss of chromatin accessibility occurred in RS, and a robust gain of chromatin accessibility occurred in OIS. The phenomenon coincided with the previous studies, the senescence-associated heterochromatin domains (SAHDs) appear partially periphery and compacted in RS, the SAHDs displace from the periphery and lose internal compaction in OIS (4). Moreover, differential SAHDs interac-

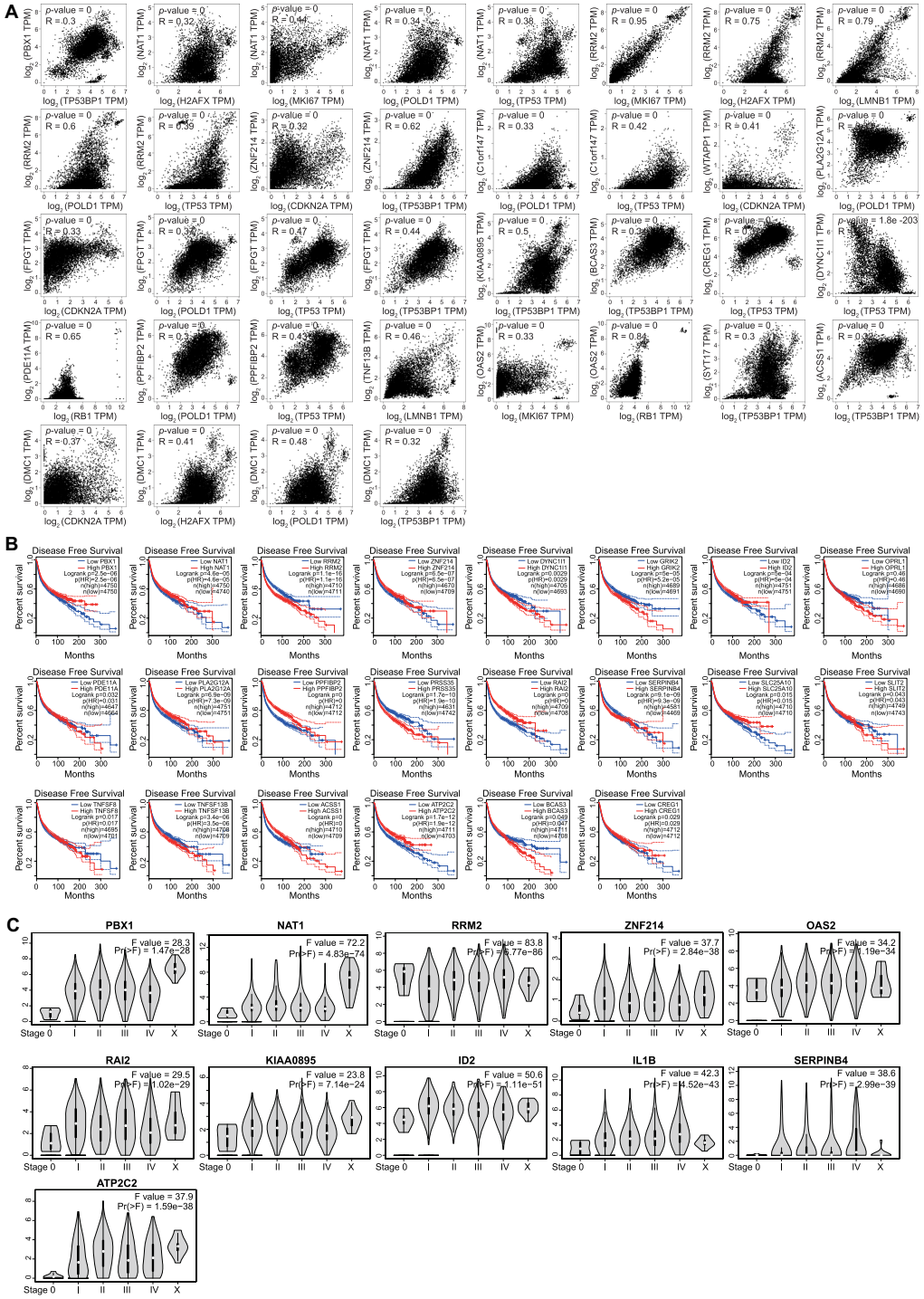

Figure 6. Appearance of 'SimultaneousAlteredGenes' in cellular senescence and agingrelated diseases. (**A**) Pearson's correlation of PBX1, NAT1, RRM2, ZNF214, C1ORF147, WTAPP1, PLA2G12A, FPGT, KIAA0895, BCAS3, CREG1, DYNC1I1, PDE11A, PPFIBP2, TNFSF13B, OAS2, SYT17, ACSS1 and DMC1 with cellular senescence markers indicated were shown, the data were extracted from GTEx database. We identified the significant correlation coefficient as P-value < 0.05 and $R > 0.3$. These genes were significantly correlated with the indicated senescent markers, the else nonsignificant results of these genes could see in Supplementary Figure S6A. The correlations of other 'SimultaneousAlteredGenes' (which were not correlated with any of the mentioned senescent markers) with senescent markers were shown in Supplementary Figure S6B. (**B**) PanCancer DFS (DiseaseFree Survival) plot of PBX1, NAT1, RRM2, ZNF214, DYNC1I1, GRIK2, ID2, OPRL1, PDE11A, PLA2G12A, PPFIBP2, PRSS35, RAI2, SERPINB4, SLC25A10, SLIT2, TNFSF8, TNFSF13B ACSS1, ATP2C2, BCAS3 and CREG1 were shown indicated. Cox proportional hazard ratio and 95% CI information were included in the survival plot. The data were analyzed by logrank test. The remaining nonsignificant genes of PanCancer DFS are shown in Supplementary Figure S6C. (**C**) PanCancer pathological stage plot of PBX1, NAT1, RRM2, ZNF214, OAS2, RAI2, KIAA0895, ID2, IL1B, SERPINB4, and ATP2C2 can been observed as indicated. The Fvalue of these genes was more than 20. The data were obtained from TCGA and GTEx (Genotype-Tissue Expression) databases. Oneway ANOVA and $\log_2$ (TPM + 1) were used for the log scale. The genes which Fvalue were less than 20 could be observed in Supplementary Figure S6D. The results of nonsignificant genes could be observed in Supplementary Figure S6E.

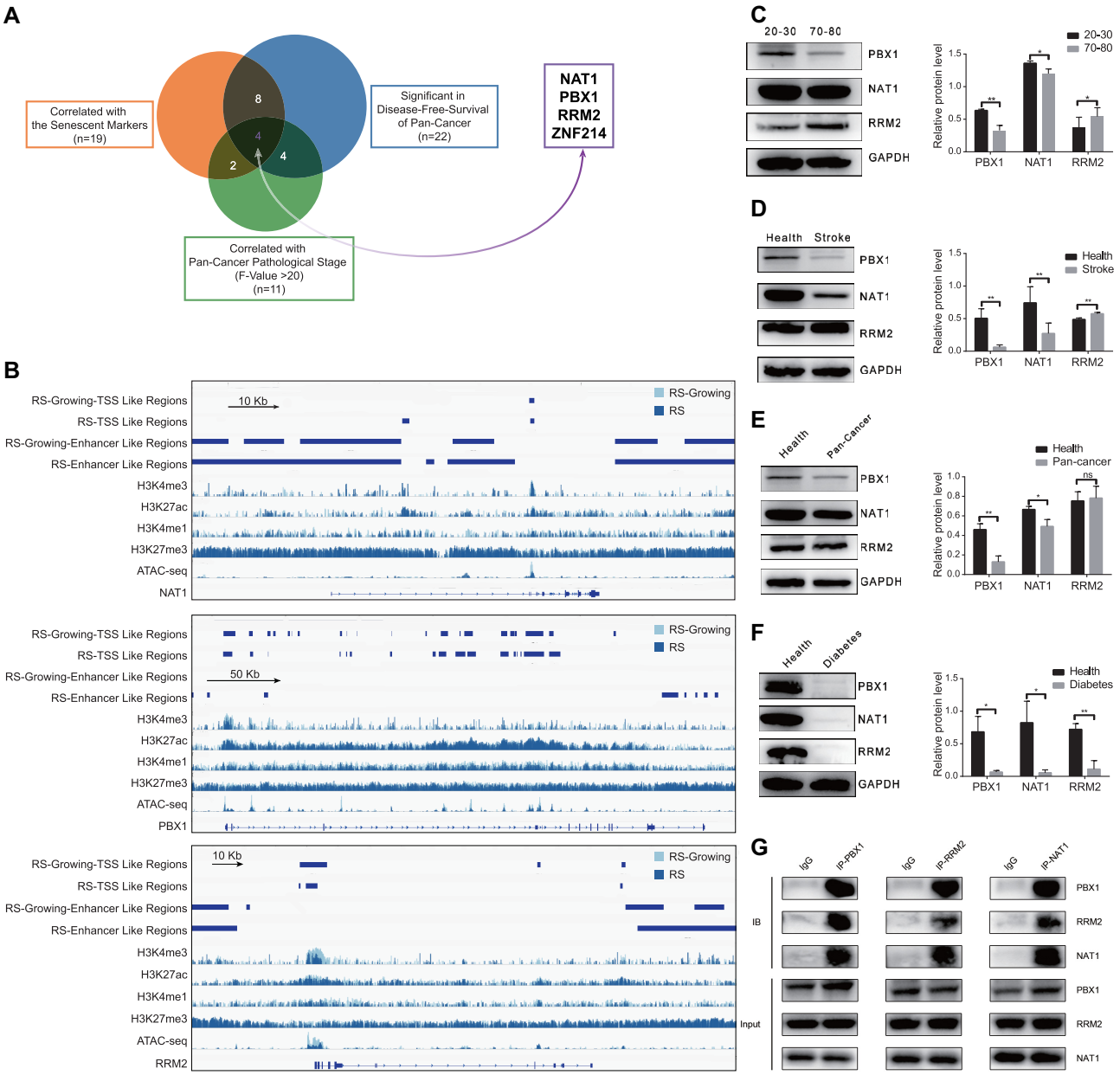

Figure 7. Integrated multiomics approach revealed that PBX1, NAT1, and RRM2 could be the new markers of cellular senescence, aging, and agingrelated diseases. (**A**) The genes, whose chromatin accessibility and expression were both altered in RS and OIS, were divided into the following three parts: those correlated with cellular senescence markers (left), those statistically significant in PanCancer DFS (right), and those statistically significant in PanCancer pathological stage (and Fvalue > 20) (bottom). The intersection of these three parts was shown in the Venn diagram. (**B**) Enrichment of NAT1, RRM2, and PBX1 in TSSlike regions (identified by H3K4me3, H3K27me3 and ATACseq), enhancerlike regions (identified by H3K4me1, H3K27ac, H3K4me3, and ATACseq), H3K4me3, H3K27me3, H3K4me1, H3K27ac and ATACseq were shown by IGV (Integrative Genomics Viewer). Light blue represents the growing cells, and dark blue indicates the RS cells. The results of OIS could also be seen in Supplementary Figure S7. The expression of NAT1, PBX1, and RRM2 in the peripheral blood mononuclear cells (PBMCs) of (**C**) the healthy people in different ages (n = 20, age = 25.3 ± 1.53 years) ($n = 20$, age = 73.25 ± 2.22 years), (**D**) patients who suffered from stroke ($n = 20$, age = 74.65 ± 3.30 years), (**E**) patients with PanCancer ($n = 20$, age = 73.05 ± 2.86 years) and (**F**) patients with diabetes ($n = 20$, age = 75.2 ± 2.33 years). (**G**) CoIP assay in healthy people PBMCs ($n = 60$, with no restriction of age) shows that PBX1, RRM2 and NAT1 can bind with each other.

tions and differential H3K9me3 marked heterochromatin led to the formation of senescence-associated heterochromatin foci (SAHFs) only in OIS, which may further account for markedly difference between RS and OIS in nuclear architecture accessibility. Meanwhile, through ChIP-seq analysis, we also obtained that, the enrichment of H3K4me1, H3K4me3, H3K27ac and H3K27me3 were decreased in RS. In the OIS, the H3K27ac, H3K27me3 were enriched less and the H3K4me1, H3K4me3 were enriched more. These results suggested the predominance of repressors over activators in senescence and explained the formation of SAHFs in the different senescent types (4,12). These consequences also explained the elevated transcriptional noise, reduced global heterochromatin, and the remodeling and loss of nucleosomes, which have only been examined in low-throughput studies (53–55). We also found that the altered chromatin accessibility in cellular senescence was always annotated in distal intergenic, intron and promoter regions, and the unchanged regions in RS were always annotated in 5′-UTR and exon regions. In general, the switch from the close to the open chromatin state leads to gene activation. Nevertheless, the increasingly altered regions annotated in distal intergenic and intron regions could lead to the noise in gene expression and the dropped rate of gene translation (56).

To investigate the association between chromatin accessibility and gene expression, we also employed the RNA-seq data of RS cells and OIS cells in the GEO database. Our results conformed to the pattern in previous studies showing that the switch between the open/closed chromatin state is associated with a pattern of differential gene expression (57,58). We then obtained 34 genes that could be the core factors of cellular senescence. To elucidate the participation of these genes in cellular senescence, aging, and aging-related disease, we employed GEPIA to analyze the data of TCGA and GTEx databases. We found 19 genes correlated with cellular senescence markers. Our findings are in agreement with some comprehensive studies showing that a few of these genes, including NAT1, PBX1, CREG1, DYNC1I1, PDE11A, TNFSF13B, BCAS3, OAS2, RRM2 and DMC1, participate in aging and aging-related diseases, such as insulin resistance, cognitive deficits, cardiovascular risk and aging-related obesity (59–69). The remaining genes, including C1ORF147, WTAPP1, PLA2G12A, FPGT, KIAA0895, PPFIBP2, SYT17, ACSS1 and ZNF214, could be the novel senescent markers. We also found 22 genes associated with the DFS of patients with Pan-Cancer and 11 genes associated with the pathological stages of Pan-Cancer. Almost all of these genes have been reported as core factors of cancer, except ZNF214 (70–92). This observation indicated that ZNF214 could be a novel marker of cancer. We also successfully identified several candidate genes from the overlap of the three independent parts, as indicated above. We deduced that the candidate intersection genes, namely, NAT1, PBX1, RRM2 and ZNF214, may play a major role as bridges between senescence and cancer. Western blot assay showed that the expression levels of NAT1 and PBX1 decreased in aging, stroke, Pan-Cancer and diabetes. We supposed that the prognosis of RRM2 at a high expression level would be bleak, and its expression fluctuated in aging and aging-related diseases. The precise mechanism of RRM2 in aging-related diseases remains unclear; additional work is needed to explore this possibility. To the best of our knowledge, the current study presented the first evidence that NAT1, PBX1 and RRM2 could interact with each other and therefore could participate in aging and aging-related diseases as protein complexes. This result supported the notion that numerous interaction networks and proteostasis network contribute to aging (52,93,94).

Following the recommendation by ENCODE, we used the integrated ATAC-seq and ChIP-seq data in the GEO database to identify novel TSS and enhancer regions (95). We also applied IGV to observe the enrichment of NAT1, PBX1, and RRM2 in ATAC-seq and ChIP-seq. We employed the integrated multi-omics approach to study the dynamic and coordinated chromatin accessibility and gene expression during senescence. The previous method used to discover enhancers relies solely on a localized enrichment of H3K4me3/H3K4me1 in intergenic regions. Here we considered that the combination of chromatin accessibility profiling and histone modification enrichment is a precise and powerful approach to identifying new trans- and cis-regulatory sequences.

Consistent with the literature, the altered genes in senescence were significantly enriched in several GO terms such as cell cycle, DNA replication, and DNA repair. These terms were similar to those enriched in ATAC-seq, RNA-seq and ChIP-seq and to the KEGG pathways. Thus, we deduced that the alteration of the cell cycle, DNA replication, and DNA repair may partly elucidate the mechanism of cellular senescence, aging, and aging-related diseases.

In summary, our work provides the landscape comprising ATAC-seq, RNA-seq and ChIP-seq to study accessibility dynamics and transcriptional regulation in cellular senescence. The application of this technique in different types of senescence allows us to identify the regulatory elements that are responsible for the temporal regulation of transcription in vivo, thus providing new insights into the molecular mechanisms of senescence (96). The challenge ahead is to apply this approach to aging-related diseases and identify ways in which these regulatory landscapes can be manipulated to control senescence and present a unique therapeutic opportunity for aging-related diseases.

DATA AVAILABILITY

The original datasets can be observed and obtained in the GEO database; the datasets can be accessible through accession number GSE210285.

SUPPLEMENTARY DATA

Supplementary Data are available at NAR Online.

ACKNOWLEDGEMENTS

We are thankful for the technical assistance of Shanghai Jiayin Biotechnology Co., Ltd. We are also grateful to PhD Liu Tong from Beijing Institute of Technology, for giving us invaluable assistance.

FUNDING

State Key Program of the National Natural Science Foundation of China [82030064]; National Natural Science Foundation of China [81871714, 81901406, 82102487]; Beijing Sail Plan for Talents Development [ZYLX202114]; Beijing Key Clinical Specialty; HUIZHI Talent Leadership Development Program of Xuanwu Hospital [HZ2021PYLJ023]. Funding for open access charge: State Key Program of the National Natural Science Foundation of China [82030064]; National Natural Science Foundation of China [81871714, 81901406, 82102487]; Beijing Sail Plan for Talents Development [ZYLX202114]; Beijing Key Clinical Specialty; HUIZHI Talent Leadership Development Program of Xuanwu Hospital [HZ2021PYLJ023].
Conflict of interest statement. None declared.

REFERENCES

1. He,S. and Sharpless,N.E. (2017) Senescence in health and disease. *Cell*, **169**, 1000–1011.
2. Calcinotto,A., Kohli,J., Zagato,E., Pellegrini,L., Demaria,M. and Alimonti,A. (2019) Cellular senescence: aging, cancer, and injury. *Physiol. Rev.*, **99**, 1047–1078.
3. Avelar,R.A., Ortega,J.G., Tacutu,R., Tyler,E.J., Bennett,D., Binetti,P., Budovsky,A., Chatsirisupachai,K., Johnson,E., Murray,A. *et al.* (2020) A multidimensional systems biology analysis of cellular senescence in aging and disease. *Genome Biol.*, **21**, 91.
4. Sati,S., Bonev,B., Szabo,Q., Jost,D., Bensadoun,P., Serra,F., Loubiere,V., Papadopoulos,G.L., Rivera-Mulia,J.C., Fritsch,L. *et al.* (2020) 4D Genome rewiring during oncogene-induced and replicative senescence. *Mol. Cell*, **78**, 522–538.
5. Uyar,B., Palmer,D., Kowald,A., Murua,E.H., Barrantes,I., Moller,S., Akalin,A. and Fuellen,G. (2020) Single-cell analyses of aging, inflammation and senescence. *Ageing Res. Rev.*, **64**, 101156.
6. Cheung,P., Vallania,F., Warsinske,H.C., Donato,M., Schaffert,S., Chang,S.E., Dvorak,M., Dekker,C.L., Davis,M.M., Utz,P.J. *et al.* (2018) Single-Cell chromatin modification profiling reveals increased epigenetic variations with aging. *Cell*, **173**, 1385–1397.
7. Martinez-Zamudio,R.I., Roux,P.F., de Freitas,J., Robinson,L., Dore,G., Sun,B., Belenki,D., Milanovic,M., Herbig,U., Schmitt,C.A. *et al.* (2020) AP-1 imprints a reversible transcriptional programme of senescent cells. *Nat. Cell Biol.*, **22**, 842–855.
8. Sen,P., Shah,P.P., Nativio,R. and Berger,S.L. (2016) Epigenetic mechanisms of longevity and aging. *Cell*, **166**, 822–839.
9. Pal,S. and Tyler,J.K. (2016) Epigenetics and aging. *Sci. Adv.*, **2**, e1600584.
10. Dang,Y., An,Y., He,J., Huang,B., Zhu,J., Gao,M., Zhang,S., Wang,X., Yang,B. and Xie,Z. (2020) Berberine ameliorates cellular senescence and extends the lifespan of mice via regulating p16 and cyclin protein expression. *Aging Cell*, **19**, e13060.
11. Wang,W., Pan,K., Chen,Y., Huang,C. and Zhang,X. (2012) The acetylation of transcription factor HBP1 by p300/CBP enhances p16INK4A expression. *Nucleic. Acids. Res.*, **40**, 981–995.
12. Parry,A.J., Hoare,M., Bihary,D., Hansel-Hertsch,R., Smith,S., Tomimatsu,K., Mannion,E., Smith,A., D'Santos,P., Russell,I.A. *et al.* (2018) NOTCH-mediated non-cell autonomous regulation of chromatin structure during senescence. *Nat. Commun.*, **9**, 1840.
13. Kudelka,M.R., Ju,T., Heimburg-Molinaro,J. and Cummings,R.D. (2015) Simple sugars to complex disease–mucin-type O-glycans in cancer. *Adv. Cancer. Res.*, **126**, 53–135.
14. Eke,I. and Cordes,N. (2015) Focal adhesion signaling and therapy resistance in cancer. *Semin. Cancer Biol.*, **31**, 65–75.
15. Swaab,D.F., Bao,A.M. and Lucassen,P.J. (2005) The stress system in the human brain in depression and neurodegeneration. *Ageing Res. Rev.*, **4**, 141–194.
16. Di Micco,R., Krizhanovsky,V., Baker,D. and D'Adda,D.F.F. (2021) Cellular senescence in ageing: from mechanisms to therapeutic opportunities. *Nat. Rev. Mol. Cell Biol.*, **22**, 75–95.
17. Hou,Y., Song,Q., Gao,S., Zhang,X., Wang,Y., Liu,J., Fu,J., Cao,M. and Wang,P. (2021) CTCF mediates replicative senescence through POLD1. *Front. Cell Dev. Biol.*, **9**, 618586.
18. Gao,S., Song,Q., Liu,J., Zhang,X., Ji,X. and Wang,P. (2019) E2F1 mediates the downregulation of POLD1 in replicative senescence. *Cell. Mol. Life Sci.*, **76**, 2833–2850.
19. Hernandez-Segura,A., de Jong,T.V., Melov,S., Guryev,V., Campisi,J. and Demaria,M. (2017) Unmasking transcriptional heterogeneity in senescent cells. *Curr. Biol.*, **27**, 2652–2660.
20. Shin,E.Y., Soung,N.K., Schwartz,M.A. and Kim,E.G. (2021) Altered endocytosis in cellular senescence. *Ageing Res. Rev.*, **68**, 101332.
21. Zirkel,A., Nikolic,M., Sofiadis,K., Mallm,J.P., Brackley,C.A., Gothe,H., Drechsel,O., Becker,C., Altmuller,J., Josipovic,N. *et al.* (2018) HMGB2 loss upon senescence entry disrupts genomic organization and induces CTCF clustering across cell types. *Mol. Cell*, **70**, 730–744.
22. Marthandan,S., Baumgart,M., Priebe,S., Groth,M., Schaer,J., Kaether,C., Guthke,R., Cellerino,A., Platzer,M., Diekmann,S. *et al.* (2016) Conserved senescence associated genes and pathways in primary human fibroblasts detected by RNA-Seq. *PLoS One*, **11**, e154531.
23. Marthandan,S., Priebe,S., Baumgart,M., Groth,M., Cellerino,A., Guthke,R., Hemmerich,P. and Diekmann,S. (2015) Similarities in gene expression profiles during in vitro aging of primary human embryonic lung and foreskin fibroblasts. *Biomed. Res. Int.*, **2015**, 731938.
24. Nelson,D.M., Jaber-Hijazi,F., Cole,J.J., Robertson,N.A., Pawlikowski,J.S., Norris,K.T., Criscione,S.W., Pchelintsev,N.A., Piscitello,D., Stong,N. *et al.* (2016) Mapping H4K20me3 onto the chromatin landscape of senescent cells indicates a function in control of cell senescence and tumor suppression through preservation of genetic and epigenetic stability. *Genome Biol.*, **17**, 158.
25. Rai,T.S., Cole,J.J., Nelson,D.M., Dikovskaya,D., Faller,W.J., Vizioli,M.G., Hewitt,R.N., Anannya,O., McBryan,T., Manoharan,I. *et al.* (2014) HIRA orchestrates a dynamic chromatin landscape in senescence and is required for suppression of neoplasia. *Genes Dev.*, **28**, 2712–2725.
26. Sen,P., Lan,Y., Li,C.Y., Sidoli,S., Donahue,G., Dou,Z., Frederick,B., Chen,Q., Luense,L.J., Garcia,B.A. *et al.* (2019) Histone acetyltransferase p300 induces de novo super-enhancers to drive cellular senescence. *Mol. Cell*, **73**, 684–698.
27. Aarts,M., Georgilis,A., Beniazza,M., Beolchi,P., Banito,A., Carroll,T., Kulisic,M., Kaemena,D.F., Dharmalingam,G., Martin,N. *et al.* (2017) Coupling shRNA screens with single-cell RNA-seq identifies a dual role for mTOR in reprogramming-induced senescence. *Genes Dev.*, **31**, 2085–2098.
28. Neyret-Kahn,H., Benhamed,M., Ye,T., Le Gras,S., Cossec,J.C., Lapaquette,P., Bischof,O., Ouspenskaia,M., Dasso,M., Seeler,J. *et al.* (2013) Sumoylation at chromatin governs coordinated repression of a transcriptional program essential for cell growth and proliferation. *Genome Res.*, **23**, 1563–1579.
29. Siebels,S., Czech-Sioli,M., Spohn,M., Schmidt,C., Theiss,J., Indenbirken,D., Gunther,T., Grundhoff,A. and Fischer,N. (2020) Merkel cell polyomavirus DNA replication induces senescence in human dermal fibroblasts in a kap1/trim28-dependent manner. *MBIO*, **11**, e00142-20.
30. Subramanian,A., Tamayo,P., Mootha,V.K., Mukherjee,S., Ebert,B.L., Gillette,M.A., Paulovich,A., Pomeroy,S.L., Golub,T.R., Lander,E.S. *et al.* (2005) Gene set enrichment analysis: a knowledge-based approach for interpreting genome-wide expression profiles. *Proc. Natl. Acad. Sci. U.S.A.*, **102**, 15545–15550.
31. Voss,T.C. and Hager,G.L. (2014) Dynamic regulation of transcriptional states by chromatin and transcription factors. *Nat. Rev. Genet.*, **15**, 69–81.
32. Shah,P.P., Donahue,G., Otte,G.L., Capell,B.C., Nelson,D.M., Cao,K., Aggarwala,V., Cruickshanks,H.A., Rai,T.S., McBryan,T. *et al.* (2013) Lamin B1 depletion in senescent cells triggers large-scale changes in gene expression and the chromatin landscape. *Genes Dev.*, **27**, 1787–1799.
33. Kirschner,K., Samarajiwa,S.A., Cairns,J.M., Menon,S., Perez-Mancera,P.A., Tomimatsu,K., Bermejo-Rodriguez,C., Ito,Y., Chandra,T., Narita,M. *et al.* (2015) Phenotype specific analyses reveal distinct regulatory mechanism for chronically activated p53. *PLos Genet.*, **11**, e1005053.

34. Chicas,A., Kapoor,A., Wang,X., Aksoy,O., Evertts,A.G., Zhang,M.Q., Garcia,B.A., Bernstein,E. and Lowe,S.W. (2012) H3K4 demethylation by jarid1a and jarid1b contributes to retinoblastoma-mediated gene silencing during cellular senescence. *Proc. Natl. Acad. Sci. U.S.A.*, **109**, 8971–8976.
35. Tasdemir,N., Banito,A., Roe,J.S., Alonso-Curbelo,D., Camiolo,M., Tschaharganeh,D.F., Huang,C.H., Aksoy,O., Bolden,J.E., Chen,C.C. *et al.* (2016) BRD4 connects enhancer remodeling to senescence immune surveillance. *Cancer Discov.*, **6**, 612–629.
36. Park,Y.K., Lee,J.E., Yan,Z., McKernan,K., O'Haren,T., Wang,W., Peng,W. and Ge,K. (2021) Interplay of BAF and MLL4 promotes cell type-specific enhancer activation. *Nat. Commun.*, **12**, 1630.
37. Frost,S.L., Liu,K., Li,I., Poulet,B., Comerford,E., De Val,S. and Bou-Gharios,G. (2018) Multiple enhancer regions govern the transcription of CCN2 during embryonic development. *J. Cell. Commun. Signal*, **12**, 231–243.
38. Cheung,I., Shulha,H.P., Jiang,Y., Matevossian,A., Wang,J., Weng,Z. and Akbarian,S. (2010) Developmental regulation and individual differences of neuronal H3K4me3 epigenomes in the prefrontal cortex. *Proc. Natl. Acad. Sci. U.S.A.*, **107**, 8824–8829.
39. Cruz,C., Della,R.M., Krueger,C., Gao,Q., Horkai,D., King,M., Field,L. and Houseley,J. (2018) Tri-methylation of histone H3 lysine 4 facilitates gene expression in ageing cells. *Elife.*, **7**, e34081.
40. Hu,C.K., Wang,W., Brind'Amour,J., Singh,P.P., Reeves,G.A., Lorincz,M.C., Alvarado,A.S. and Brunet,A. (2020) Vertebrate diapause preserves organisms long term through polycomb complex members. *Science*, **367**, 870–874.
41. Ma,Z., Wang,H., Cai,Y., Wang,H., Niu,K., Wu,X., Ma,H., Yang,Y., Tong,W., Liu,F. *et al.* (2018) Epigenetic drift of H3K27me3 in aging links glycolysis to healthy longevity in drosophila. *Elife.*, **7**, e35368.
42. Benayoun,B.A., Pollina,E.A., Singh,P.P., Mahmoudi,S., Harel,I., Casey,K.M., Dulken,B.W., Kundaje,A. and Brunet,A. (2019) Remodeling of epigenome and transcriptome landscapes with aging in mice reveals widespread induction of inflammatory responses. *Genome Res.*, **29**, 697–709.
43. Tang,Z., Li,C., Kang,B., Gao,G., Li,C. and Zhang,Z. (2017) GEPIA: a web server for cancer and normal gene expression profiling and interactive analyses. *Nucleic Acids Res.*, **45**, W98–W102.
44. Kansara,M., Leong,H.S., Lin,D.M., Popkiss,S., Pang,P., Garsed,D.W., Walkley,C.R., Cullinane,C., Ellul,J., Haynes,N.M. *et al.* (2013) Immune response to RB1-regulated senescence limits radiation-induced osteosarcoma formation. *J. Clin. Invest.*, **123**, 5351–5360.
45. Filippi-Chiela,E.C., Bueno,E.S.M., Thome,M.P. and Lenz,G. (2015) Single-cell analysis challenges the connection between autophagy and senescence induced by DNA damage. *Autophagy*, **11**, 1099–1113.
46. Mathews,K.J., Allen,K.M., Boerrigter,D., Ball,H., Shannon,W.C. and Double,K.L. (2017) Evidence for reduced neurogenesis in the aging human hippocampus despite stable stem cell markers. *Aging Cell*, **16**, 1195–1199.
47. Wang,L., Xu,C., Johansen,T., Berger,S.L. and Dou,Z. (2021) SIRT1 - a new mammalian substrate of nuclear autophagy. *Autophagy*, **17**, 593–595.
48. Parnandi,N., Rendo,V., Cui,G., Botuyan,M.V., Remisova,M., Nguyen,H., Drane,P., Beroukhim,R., Altmeyer,M., Mer,G. *et al.* (2021) TIRR inhibits the 53BP1-p53 complex to alter cell-fate programs. *Mol. Cell*, **81**, 2583–2595.
49. Shah,Y., Verma,A., Marderstein,A.R., White,J., Bhinder,B., Garcia,M.J. and Elemento,O. (2021) Pan-cancer analysis reveals molecular patterns associated with age. *Cell Rep.*, **37**, 110100.
50. Campbell,P.J., Getz,G., Korbel,J.O., Stuart,J.M., Jennings,J.L., Stein,L.D., Perry,M.D., Nahal-Bose,H.K., Ouellette,B.F.F., Li,C.H. *et al.* (2020) Pan-cancer analysis of whole genomes. *Nature*, **578**, 82–93.
51. Yan,F., Powell,D.R., Curtis,D.J. and Wong,N.C. (2020) From reads to insight: a hitchhiker's guide to ATAC-seq data analysis. *Genome Biol.*, **21**, 22.
52. Morris,B.J., Willcox,B.J. and Donlon,T.A. (2019) Genetic and epigenetic regulation of human aging and longevity. *Biochim. Biophys. Acta. Mol. Basis Dis.*, **1865**, 1718–1744.
53. Ecker,S., Pancaldi,V., Valencia,A., Beck,S. and Paul,D.S. (2018) Epigenetic and transcriptional variability shape phenotypic plasticity. *Bioessays*, **40**, 1700148.
54. Kane,A.E. and Sinclair,D.A. (2019) Epigenetic changes during aging and their reprogramming potential. *Crit. Rev. Biochem. Mol. Biol.*, **54**, 61–83.
55. Zhang,W., Li,J., Suzuki,K., Qu,J., Wang,P., Zhou,J., Liu,X., Ren,R., Xu,X., Ocampo,A. *et al.* (2015) Aging stem cells. A werner syndrome stem cell model unveils heterochromatin alterations as a driver of human aging. *Science*, **348**, 1160–1163.
56. Raj,A. and van Oudenaarden,A. (2008) Nature, nurture, or chance: stochastic gene expression and its consequences. *Cell*, **135**, 216–226.
57. Wang,Y., Zhang,X., Song,Q., Hou,Y., Liu,J., Sun,Y. and Wang,P. (2020) Characterization of the chromatin accessibility in an alzheimer's disease (AD) mouse model. *Alzheimers Res. Ther.*, **12**, 29.
58. Ruiz,J.L., Tena,J.J., Bancells,C., Cortes,A., Gomez-Skarmeta,J.L. and Gomez-Diaz,E. (2018) Characterization of the accessible genome in the human malaria parasite plasmodium falciparum. *Nucleic. Acids. Res.*, **46**, 9414–9431.
59. Barker,D.F., Walraven,J.M., Ristagno,E.H., Doll,M.A., States,J.C. and Hein,D.W. (2008) Quantitative tissue and gene-specific differences and developmental changes in nat1, nat2, and nat3 mRNA expression in the rat. *Drug Metab. Dispos.*, **36**, 2445–2451.
60. Hansen,R.K., Mund,A., Poulsen,S.L., Sandoval,M., Klement,K., Tsouroula,K., Tollenaere,M.A., Raschle,M., Soria,R., Offermanns,S. *et al.* (2016) SCAI promotes DNA double-strand break repair in distinct chromosomal contexts. *Nat. Cell Biol.*, **18**, 1357–1366.
61. Hashimoto,M., Goto,A., Endo,Y., Sugimoto,M., Ueda,J. and Yamashita,H. (2021) Effects of CREG1 on age-associated metabolic phenotypes and renal senescence in mice. *Int. J. Mol. Sci.*, **22**, 1276.
62. Kim,B. and Hyun,C.K. (2020) B-Cell-Activating factor depletion ameliorates aging-dependent insulin resistance via enhancement of thermogenesis in adipose tissues. *Int. J. Mol. Sci.*, **21**, 5121.
63. Liu,F., Shi,J., Zhang,Y., Lian,A., Han,X., Zuo,K., Liu,M., Zheng,T., Zou,F., Liu,X. *et al.* (2019) NANOG attenuates hair follicle-derived mesenchymal stem cell senescence by upregulating PBX1 and activating AKT signaling. *Oxid. Med. Cell Longev.*, **2019**, 4286213.
64. Liu,Z.D., Zhang,S., Hao,J.J., Xie,T.R. and Kang,J.S. (2016) Cellular model of neuronal atrophy induced by DYNC1I1 deficiency reveals protective roles of RAS-RAF-MEK signaling. *Protein Cell*, **7**, 638–650.
65. Lopez-Contreras,A.J., Specks,J., Barlow,J.H., Ambrogio,C., Desler,C., Vikingsson,S., Rodrigo-Perez,S., Green,H., Rasmussen,L.J., Murga,M. *et al.* (2015) Increased rrm2 gene dosage reduces fragile site breakage and prolongs survival of ATR mutant mice. *Genes Dev.*, **29**, 690–695.
66. Patel,M.V., Hopkins,D.C., Barr,F.D. and Wira,C.R. (2021) Sex hormones and aging modulate interferon lambda 1 production and signaling by human uterine epithelial cells and fibroblasts. *Front. Immunol.*, **12**, 718380.
67. Pilarzyk,K., Klett,J., Pena,E.A., Porcher,L., Smith,A.J. and Kelly,M.P. (2019) Loss of function of phosphodiesterase 11A4 shows that recent and remote long-term memories can be uncoupled. *Curr. Biol.*, **29**, 2307–2321.
68. Rastogi,T., Girerd,N., Lamiral,Z., Bresso,E., Bozec,E., Boivin,J.M., Rossignol,P., Zannad,F. and Ferreira,J.P. (2022) Impact of smoking on cardiovascular risk and premature ageing: findings from the STANISLAS cohort. *Atherosclerosis*, **346**, 1–9.
69. Zheng,J.S., Luan,J., Sofianopoulou,E., Imamura,F., Stewart,I.D., Day,F.R., Pietzner,M., Wheeler,E., Lotta,L.A., Gundersen,T.E. *et al.* (2021) Plasma vitamin c and type 2 diabetes: genome-wide association study and mendelian randomization analysis in european populations. *Diabetes Care.*, **44**, 98–106.
70. Cho,J.W., Hong,M.H., Ha,S.J., Kim,Y.J., Cho,B.C., Lee,I. and Kim,H.R. (2020) Genome-wide identification of differentially methylated promoters and enhancers associated with response to anti-PD-1 therapy in non-small cell lung cancer. *Exp. Mol. Med.*, **52**, 1550–1563.
71. Dhaini,H.R., El,H.B. and Khamis,A.M. (2018) NAT1 genotypic and phenotypic contribution to urinary bladder cancer risk: a systematic review and meta-analysis. *Drug Metab. Rev.*, **50**, 208–219.
72. Hlouschek,J., Ritter,V., Wirsdorfer,F., Klein,D., Jendrossek,V. and Matschke,J. (2018) Targeting SLC25A10 alleviates improved antioxidant capacity and associated radioresistance of cancer cells induced by chronic-cycling hypoxia. *Cancer Lett.*, **439**, 24–38.
73. Jang,J.H., Kim,D.H., Lim,J.M., Lee,J.W., Jeong,S.J., Kim,K.P. and Surh,Y.J. (2020) Breast cancer cell-derived soluble CD44 promotes

tumor progression by triggering macrophage IL1beta production. *Cancer Res.*, **80**, 1342–1356.
74. Tavora,B., Mederer,T., Wessel,K.J., Ruffing,S., Sadjadi,M., Missmahl,M., Ostendorf,B.N., Liu,X., Kim,J.Y., Olsen,O. *et al.* (2020) Tumoural activation of TLR3-SLIT2 axis in endothelium drives metastasis. *Nature*, **586**, 299–304.
75. Zhang,Y. and Yu,C. (2020) Prognostic characterization of OAS1/OAS2/OAS3/OASL in breast cancer. *BMC Cancer*, **20**, 575.
76. Veiga,R.N., de Oliveira,J.C. and Gradia,D.F. (2021) PBX1: a key character of the hallmarks of cancer. *J. Mol. Med. (Berl.)*, **99**, 1667–1680.
77. Wang,J., Xu,Y., Chen,Z., Liang,J., Lin,Z., Liang,H., Xu,Y., Wu,Q., Guo,X., Nie,J. *et al.* (2020) Liver immune profiling reveals pathogenesis and therapeutics for biliary atresia. *Cell*, **183**, 1867–1883.
78. Yang,Y., Lin,J., Guo,S., Xue,X., Wang,Y., Qiu,S., Cui,J., Ma,L., Zhang,X. and Wang,J. (2020) RRM2 protects against ferroptosis and is a tumor biomarker for liver cancer. *Cancer Cell Int.*, **20**, 587.
79. Liang,Z.Z., Zhang,Y.X., Zhu,R.M., Li,Y.L., Jiang,H.M., Li,R.B., Chen,Q.X., Wang,Q., Tang,L.Y. and Ren,Z.F. (2022) Identification of epigenetic modifications mediating the antagonistic effect of selenium against cadmium-induced breast carcinogenesis. *Environ. Sci. Pollut. Res. Int.*, **29**, 22056–22068.
80. Berg,M., Agesen,T.H., Thiis-Evensen,E., Merok,M.A., Teixeira,M.R., Vatn,M.H., Nesbakken,A., Skotheim,R.I. and Lothe,R.A. (2010) Distinct high resolution genome profiles of early onset and late onset colorectal cancer integrated with gene expression data identify candidate susceptibility loci. *Mol. Cancer*, **9**, 100.
81. Clark,D.J., Mei,Y., Sun,S., Zhang,H., Yang,A.J. and Mao,L. (2016) Glycoproteomic approach identifies KRAS as a positive regulator of CREG1 in Non-small cell lung cancer cells. *Theranostics.*, **6**, 65–77.
82. Gao,X., Lin,S.H., Ren,F., Li,J.T., Chen,J.J., Yao,C.B., Yang,H.B., Jiang,S.X., Yan,G.Q., Wang,D. *et al.* (2016) Acetate functions as an epigenetic metabolite to promote lipid synthesis under hypoxia. *Nat. Commun.*, **7**, 11960.
83. Koch,L. (2011) Cancer: PDE11a-a phenotype modifier in carney complex. *Nat. Rev. Endocrinol.*, **7**, 64.
84. Lake,S.L., Jmor,F., Dopierala,J., Taktak,A.F., Coupland,S.E. and Damato,B.E. (2011) Multiplex ligation-dependent probe amplification of conjunctival melanoma reveals common BRAF V600E gene mutation and gene copy number changes. *Invest. Ophthalmol. Vis. Sci.*, **52**, 5598–5604.
85. Liu,J., Wei,Y., Wu,Y., Li,J., Sun,J., Ren,G. and Li,H. (2021) ATP2C2 has potential to define tumor microenvironment in breast cancer. *Front. Immunol.*, **12**, 657950.
86. Masoud,G.N. and Li,W. (2015) HIF-1alpha pathway: role, regulation and intervention for cancer therapy. *Acta Pharm. Sin. B.*, **5**, 378–389.
87. Miyata,H., Hirohashi,Y., Yamada,S., Yanagawa,J., Murai,A., Hashimoto,S., Tokita,S., Hori,K., Abe,T., Kubo,T. *et al.* (2022) GRIK2 is a target for bladder cancer stem-like cell-targeting immunotherapy. *Cancer Immunol. Immunother.*, **71**, 795–806.
88. Sakthikumar,S., Roy,A., Haseeb,L., Pettersson,M.E., Sundstrom,E., Marinescu,V.D., Lindblad-Toh,K. and Forsberg-Nilsson,K. (2020) Whole-genome sequencing of glioblastoma reveals enrichment of non-coding constraint mutations in known and novel genes. *Genome Biol.*, **21**, 127.
89. Van Hove,L., Lecomte,K., Roels,J., Vandamme,N., Vikkula,H.K., Hoorens,I., Ongenae,K., Hochepied,T., Donati,G., Saeys,Y. *et al.* (2021) Fibrotic enzymes modulate wound-induced skin tumorigenesis. *EMBO Rep.*, **22**, e51573.
90. Wang,M., Takahashi,A., Liu,F., Ye,D., Ding,Q., Qin,C., Yin,C., Zhang,Z., Matsuda,K., Kubo,M. *et al.* (2015) Large-scale association analysis in asians identifies new susceptibility loci for prostate cancer. *Nat. Commun.*, **6**, 8469.
91. Werner,S., Brors,B., Eick,J., Marques,E., Pogenberg,V., Parret,A., Kemming,D., Wood,A.W., Edgren,H., Neubauer,H. *et al.* (2015) Suppression of early hematogenous dissemination of human breast cancer cells to bone marrow by retinoic Acid-induced 2. *Cancer Discov.*, **5**, 506–519.
92. Markovina,S., Wang,S., Henke,L.E., Luke,C.J., Pak,S.C., DeWees,T., Pfeifer,J.D., Schwarz,J.K., Liu,W., Chen,S. *et al.* (2018) Serum squamous cell carcinoma antigen as an early indicator of response during therapy of cervical cancer. *Br. J. Cancer*, **118**, 72–78.
93. Hipp,M.S., Kasturi,P. and Hartl,F.U. (2019) The proteostasis network and its decline in ageing. *Nat. Rev. Mol. Cell Biol.*, **20**, 421–435.
94. Khan,S.S., Singer,B.D. and Vaughan,D.E. (2017) Molecular and physiological manifestations and measurement of aging in humans. *Aging Cell*, **16**, 624–633.
95. The ENCODE Project Consortium (2012) An integrated encyclopedia of DNA elements in the human genome. *Nature*, **489**, 57–74.
96. Struckmann,S., Ernst,M., Fischer,S., Mah,N., Fuellen,G. and Moller,S. (2021) Scoring Functions for Drug-effect Similarity. *Brief Bioinform*, **22**, bbaa072.